

1 **Unified neural pathways that gate affective pain and**
2 **multisensory innate threat signals to the amygdala**

3
4

5 Sukjae Joshua Kang^{1,5}, Shijia Liu^{1,2,5}, Mao Ye^{1,5}, Dong-Il Kim¹, Jong-Hyun Kim¹, Tae Gyu Oh³, Jiahang
6 Peng^{1,2}, Ronald M. Evans³, Kuo-Fen Lee¹, Martyn Goulding⁴, Sung Han^{1,2}. *

7

8 1 Peptide Biology Laboratories, The Salk Institute for Biological Studies, La Jolla, CA 92037, USA

9 2 Section of Neurobiology, Division of Biological Sciences, University of California, San Diego, La Jolla,
10 CA 92093, USA

11 3 Howard Hughes Medical Institute, Gene Expression Laboratories, The Salk Institute for Biological
12 Studies, La Jolla, CA 92037, USA

13 4 Molecular Neurobiology Laboratories, The Salk Institute for Biological Studies, La Jolla, CA 92037,
14 USA

15 5 Co-first authors

16

17

18

19

20 *Correspondence to:

21 Sung Han, Ph.D.

22 Peptide Biology Laboratories,

23 Salk Institute for Biological Studies

24 10010 N. Torrey Pines Rd.

25 La Jolla, CA 92037, USA

26 Email: sunghan@salk.edu

27 Phone: (858) 453-4100, x1856

28

29 **Abstract**

30 Perception of aversive sensory stimuli such as pain and innate threat cues is essential for animal survival.
31 The amygdala is critical for aversive sensory perception, and it has been suggested that multiple parallel
32 pathways independently relay aversive cues from each sensory modality to the amygdala. However, a
33 convergent pathway that relays all aversive sensory cues to the amygdala has not been identified. Here, we
34 report that neurons expressing calcitonin gene-related peptide (CGRP) in the parvocellular subparafasicular
35 thalamic nucleus (SPFp) are necessary and sufficient for affective-motivational pain perception by forming
36 a spino-thalamo-amygdaloid pain pathway. In addition, we find that this CGRP pathway, together with the
37 parabrachio-amygdaloid CGRP pathway, is critical for the perception of threat stimuli from all sensory
38 modalities. The discovery of unified pathways that collectively gate aversive sensory stimuli from all
39 sensory modalities may provide critical circuit-based insights for developing therapeutic interventions for
40 affective pain- and innate fear-related disorders.

41 **Introduction**

42 Pain is a complex sensory and emotional experience caused by tissue-damaging noxious stimuli that
43 produce immediate avoidance behavior, as well as long-lasting aversive memories so that future damage
44 can be avoided (Julius and Basbaum, 2001; Melzack and Casey, 1968). Therefore, the perception of pain
45 results in behavioral outcomes similar to those associated with the perception of threats. Indeed, most
46 research on Pavlovian threat learning has used electric foot shock, a painful noxious stimulus, as a threat
47 cue. It has also been suggested that pain and threat perceptions interact with each other (Elman and Borsook,
48 2018). Individuals with pain asymbolia, who have deficits in perceiving affective and motivational aspects
49 of pain due to damage to limbic structures, show compromised perception of threats (Berthier et al., 1988).
50 Alternatively, people with affective pain disorders, such as migraine and fibromyalgia, are often
51 hypersensitive to sensory inputs and perceive normal sensory signals as threats (Bar-Shalita et al., 2019;
52 López-Solà et al., 2017). Therefore, it is likely that there are unified neural circuits and brain areas that
53 process both pain-causing noxious stimuli and threat-producing aversive sensory cues (Price, 1999).

54
55 The amygdala is a key limbic structure that integrates sensory stimuli with an internal state to generate
56 appropriate emotional responses (Janak and Tye, 2015; LeDoux, 2012, 2000). It is activated by aversive
57 sensory stimuli, including noxious stimuli (Ren and Neugebauer, 2010; Simons et al., 2014; Veinante et al.,
58 2013), and lesioning the amygdala greatly attenuates the perception of multimodal sensory threats (Bach et
59 al., 2015; Blanchard and Blanchard, 1972; Dal Monte et al., 2015) and pain (Gao et al., 2004; Helmstetter,
60 1992; Manning and Mayer, 1995; Tanimoto et al., 2003). Therefore, the amygdala may serve as a pivotal
61 node in integrating and unifying all threat cues from different sensory modalities, including pain-causing
62 noxious stimuli. Recent studies suggest that aversive sensory stimuli from each sensory modality relay
63 threat cues to the amygdala through parallel non-overlapping pathways. These include somatosensory
64 (Barsy et al., 2020; Choi et al., 2020; Han et al., 2015; Sato et al., 2015), visual (Salay et al., 2018; Wei et
65 al., 2015; Zhou et al., 2019), auditory (Barsy et al., 2020), gustatory (Carter et al., 2013; Kim et al., 2017;
66 Wang et al., 2018) and olfactory (Rosen et al., 2015; Tong et al., 2020). However, little is known about the
67 convergent neural circuits that relay and integrate multimodal aversive sensory signals, including
68 nociceptive signals, to the amygdala.

69
70 Noxious stimuli from the periphery are relayed to the brain through two ascending pain pathways, the spino-
71 parabrachial pathway and the spino-thalamic pathway (Bushnell et al., 2013). It is a well-established idea
72 that the spino-thalamic pathway is involved in sensory and discriminative pain perception and that the spino-
73 parabrachial pathway is involved in the perception of affective and motivational pain. This is because the
74 former projects to the somatosensory cortex and the latter projects to the amygdala (Basbaum et al., 2009).
75 Among multiple areas of the amygdala, the capsular subdivision of the central nucleus of the amygdala
76 (CeC) is known as the nociceptive amygdala since it is activated by nociceptive stimuli and receives direct
77 input from the parabrachial nucleus (PBN) through the spino-parabrachial pathway (Gauriau and Bernard,
78 2002; Neugebauer, 2015). Nevertheless, it remains unclear which types of nociceptive information are
79 relayed to other areas of the amygdala involved in pain processing, such as the amygdala-striatum transition
80 area (AStr) (Xiu et al., 2014) and the lateral nucleus of the amygdala (LA) (Bernard et al., 1992; Corder et
81 al., 2019; Thompson and Neugebauer, 2017). In particular, the LA is critically involved in pain-induced
82 aversive learning (LeDoux, 2007; Ressler and Maren, 2019), but the detailed pain pathway that relays
83 nociceptive information to the LA has not been fully understood.

84

85 Although the thalamus has been implicated in sensory and discriminative pain (Dado et al., 1994; Zhang
86 and Giesler, 2005), some thalamic nuclei, such as the ventromedial posterior thalamus (VMpo) in primates,
87 or the triangular subdivision of the posterior thalamus (PoT) in rodents, are thought to be involved in
88 affective and motivational pain perception by relaying nociceptive signals to the insular cortex (Craig et al.,
89 2000; Gauriau and Bernard, 2004a; Price, 2002; Willis et al., 2002). However, the involvement of these
90 nuclei in affective and motivational pain perception is still inconclusive, mainly because the thalamus has
91 many small, functionally distinct nuclei without clear anatomical boundaries. Therefore, to understand the
92 roles of the thalamus in affective pain processing, it is critical to identify genetically defined populations of
93 thalamic neurons that play specific roles in this process.

94

95 Calcitonin gene-related peptide (CGRP) is a 37-amino acid neuropeptide produced by peripheral neurons
96 and mediates vasodilation and nociceptive transmission (Russell et al., 2014; Russo, 2015). It is also
97 produced in the brain and plays an essential role in aversive learning and pain perception (Palmiter, 2018;
98 Shinohara et al., 2017; Yu et al., 2009). CGRP-expressing neurons are highly clustered in two brain areas:
99 the external lateral subdivision of the PBN (PBel) and the parvocellular subparafascicular nucleus (SPFp)
100 (D'Hanis et al., 2007; Dobolyi et al., 2005); (Experiment 79587715, Allen Brain Atlas). Previous studies
101 have shown that CGRP neurons in the PBel (CGRP^{PBel}) are critically involved in transmitting affective pain
102 signals during aversive learning (Han et al., 2015) and in transmitting visceral aversive signals to the CeA
103 (Chen et al., 2018). On the other hand, the latter is a relatively unexplored area. The SPFp is an elongated
104 structure that extends from the anteromedial to posterolateral thalamus (D'Hanis et al., 2007). It has been
105 speculated that CGRP neurons in the medial part of the SPFp (CGRP^{SPFp}) may play a role in sexual
106 behaviors (Coolen et al., 2003a, 2003b), whereas those in the posterolateral part of the CGRP^{SPFp} may be
107 involved in emotional behaviors, based on anatomical projections to the amygdala (D'Hanis et al., 2007;
108 LeDoux et al., 1985; Yasui et al., 1991). However, this idea has not been tested. Furthermore, it is unknown
109 to what extent CGRP^{PBel} and CGRP^{SPFp} neurons play similar roles in conveying aversive sensory
110 information to the amygdala.

111

112 Here, we report that CGRP^{SPFp} neurons receive direct monosynaptic inputs from projection neurons within
113 the dorsal horn of the spinal cord and project their axons to multiple regions within the amygdala (namely
114 the AStr and the LA) and to the posterior insular cortex, but not to the somatosensory cortex. These neurons
115 are activated by multimodal nociceptive stimuli. Silencing these neurons substantially attenuates affective
116 and motivational pain perception, and activating these neurons induces aversion and aversive memory.
117 Furthermore, CGRP^{SPFp} neurons, together with CGRP^{PBel} neurons, are collectively activated by aversive
118 sensory stimuli from all sensory modalities (visual, auditory, somatosensory, gustatory, and olfactory), and
119 silencing these neurons attenuates the perception of all aversive sensory stimuli. Taken together, CGRP
120 neurons within the SPFp and PBel not only form two affective pain pathways for relaying affective-
121 motivation pain, namely the spino-thalamo-amygdaloid and the spino-parabracho-amygdaloid pathways,
122 but they also relay aversive sensory signals from all sensory modalities to the amygdala during threat
123 perception.

124

125 **Results**

126 **CGRP^{SPFp} and CGRP^{PBel} neurons relay multisensory inputs from sensory modalities to the amygdala**

127 The amygdala is critically involved in the affective-motivational pain perception. However, it is not fully
128 understood by which the nociceptive information is conveyed to the amygdala. Nociceptive information is
129 encoded by spinal cord neurons that send a number of specific projections to the brain (Basbaum et al.,
130 2009; Todd, 2010). One example is spinal projection neurons within the superficial layer of the spinal dorsal
131 horn that express the *Tacr1* gene (Barik et al., 2020; Chiang et al., 2020; Choi et al., 2020; Deng et al.,
132 2020). To identify direct spino-recipient areas in the brain, we genetically labeled only the spinal *Tacr1*
133 neurons with tdTomato fluorescent protein by the triple crossing of *Tacr1^{Cre}*, *Cdx2^{FlpO}*, and *Ai65* (Rosa-
134 CAG-FrtSTOPFrt-LoxSTOPLox-tdTomato; *dsTomato*) mice as described previously (Bourane et al., 2015)
135 (Figure S1A). The tdTomato-expressing cell bodies were only observed in the spinal dorsal horn (Figure
136 S1A). Fluorescently labeled axonal terminals were observed in multiple brain areas, including the PBN,
137 SPFp, the posterior complex of the thalamus (Po), the ventral posterolateral nucleus of the thalamus (VPL),
138 superior colliculus (SC), periaqueductal gray (PAG), dorsal column nuclei (DCN), and ventrolateral
139 medulla (VLM) (Figure S1B). We then asked which of these areas project to the amygdala. By searching
140 through the Allen Mouse Connectivity Atlas (<http://connectivity.brain-map.org/>), we found that the SPFp
141 and PBel project to the LA and CeA, respectively. Interestingly, CGRP neurons are found in both the SPFp
142 and PBel, and CGRP^{PBel} neurons are known to play a role in affective pain perception (Han et al., 2015).
143 Therefore, we sought to dissect and compare the roles of these CGRP circuits in processing nociceptive
144 sensory information and relaying this information to the amygdala.

145 To identify regions that lie downstream of CGRP neurons in the SPFp and PBel, we injected Cre-
146 dependent AAVs encoding EYFP or mCherry into the SPFp and PBel of the *Calca^{Cre}* mouse that expresses
147 Cre-recombinase in the CGRP-expressing neurons (*Calca* gene encodes CGRP), respectively (Figure 1A).
148 Coronal slices around AP -1.1 showed an intermingled green and red expression pattern in the CeA and LA
149 (Figure S2A). However, posterior slices (AP -1.5) revealed distinct patterns of EYFP and mCherry in the
150 amygdala. While the CGRP^{SPFp} synaptic terminals were found in the AStr, LA, and medial amygdala
151 (MEA), the CGRP^{PBel} terminals were most abundant in the CeA, and basomedial amygdala (BMA) (Figure
152 1B). CGRP^{SPFp} neurons also projected to the auditory cortex and the dorsal regions of the posterior insular
153 cortex (pIC), whereas CGRP^{PBel} neurons projected to the bed nuclei of the stria terminalis (BNST), ventral
154 posteromedial nucleus of the thalamus parvicellular part (VPMpc), parasubthalamic nucleus (PSTN), and
155 the ventral portion of the pIC (Figure S2B).

156 To identify upstream brain regions that directly project their axons to the CGRP^{SPFp}, or CGRP^{PBel} neurons,
157 we performed cell-type-specific monosynaptic retrograde tracing using pseudotyped rabies virus (Kim et
158 al., 2016). We injected AAV8-hSyn-FLEX-TVA-P2A-GFP-2A-oG into the SPFp or PBel of *Calca^{Cre}* mice
159 and then waited three weeks before injecting EnvA-ΔG-rabies-mCherry into the same region (Figure 1C).
160 Five days later, mice were sacrificed, and starter cells were observed in both regions (Figure 1D). Within
161 the spinal cord (Figure 1E), histological analyses revealed that CGRP^{SPFp} neurons received inputs from
162 different layers of the spinal cord (Figures 1F, and G), but most abundantly from the cervical segment
163 (Figure 1H). By contrast, fewer neurons in the spinal cord projected to the CGRP^{PBel} neurons compared to
164 those projecting to the CGRP^{SPFp} neurons (Figures 1I-K). Other than the spinal cord, CGRP^{SPFp} neurons
165 received inputs from sensory relay areas including the SC, inferior colliculus (IC), vestibular nucleus (VN),
166 and trigeminal spinal nucleus (SpV), as well as other regions such as the hypothalamus and cortex (Figures
167 S3A, C, and E). The strongest inputs to CGRP^{PBel} neurons were derived from the amygdala (in particular
168 the CeA) and the hypothalamus (including the lateral hypothalamus (LHA), zona inserta (ZI), and PSTN)

169 (Figures S3B, D, and F). CGRP^{PBel} neurons also received projections from sensory relay areas, including
170 the SC, IC, VN, and SpV. Thus, these two populations of CGRP neurons received input from several
171 sensory relay regions in common.

172 Our results show that both CGRP^{SPFp} and CGRP^{PBel} neurons receive monosynaptic inputs from the spinal
173 dorsal horn, other sensory-related regions, hypothalamus, and amygdala (CGRP^{PBel} neurons in particular).
174 However, in terms of output patterns, CGRP^{SPFp} neurons project to the LA and AStr, while CGRP^{PBel}
175 neurons project to the CeA, thereby forming complementary parallel sensory pathways to the amygdala.

176

177 **CGRP^{SPFp} and CGRP^{PBel} neurons are activated by multimodal nociceptive stimuli**

178 Next, we investigated the response of CGRP^{SPFp} and CGRP^{PBel} neurons to multimodal nociceptive stimuli,
179 such as mechanical, thermal, and inflammatory stimuli by the fiber photometry *in vivo* calcium monitoring
180 technique (Figure 2A). AAV-DIO-GCaMP6m was injected into the SPFp or PBel of *Calca^{Cre}* mice, and an
181 optic fiber (400 μ m, 0.37 NA) was implanted above the injection site (Figures 2B, and C). Previous *in vivo*
182 electrophysiology studies have shown that nociceptive signals can be conveyed to the spinal cord and brain
183 under anesthesia (Gauriau and Bernard, 2004b; Peschanski et al., 1981). Therefore, we performed the fiber
184 photometry experiments under light anesthesia to remove other emotional confounding factors.

185 Various intensities of mechanical stimuli (0, 50, 100, 200, and 300 g of pressure delivered by a pressure
186 meter, not von Frey hair) were applied for 5 seconds to the ipsi- or contra-lateral paws or tail, resulting in
187 intensity-dependent increases in calcium signals (Area under curve analysis; A.U.C.) in both CGRP^{SPFp}
188 (Figures 2D-F) and CGRP^{PBel} neurons (Figures 2G-I), but here was significantly decreased calcium
189 response in the CGRP^{PBel} neurons by 300 g stimulation which created the inverted U-shaped intensity
190 response curve. Nevertheless, CGRP^{SPFp} and CGRP^{PBel} neurons display different dynamics to noxious
191 stimuli. CGRP^{PBel} neurons reached maximum response at lower stimulation intensity compared to the
192 CGRP^{SPFp} neurons (Figures S4A, and B), but the latter responded faster to the stimuli, which was observed
193 by greater initial rise slope of calcium peak in the CGRP^{SPFp} neurons compared to the CGRP^{PBel} neurons
194 (Figure S4C). Although contralateral stimulation evoked greater responses than the ipsilateral stimulation,
195 both the CGRP^{SPFp} and CGRP^{PBel} neurons were activated by noxious stimuli from both side, contrary to the
196 conventional lateralized ascending sensory pain pathways. (Figures S4D-G).

197 Heat stimuli (25, 35, 45, and 55°C) also induced intensity-dependent calcium increases in both CGRP^{SPFp}
198 (Figure 2J-L) and CGRP^{PBel} neurons (Figure 2M-O). The maximum calcium peak values were higher
199 overall in CGRP^{PBel} neurons than in CGRP^{SPFp} neurons, both for contralateral (Figure S4H) and ipsilateral
200 stimulations (Figure S4I). However, the CGRP^{SPFp} neurons again responded faster to 55 °C stimuli than
201 CGRP^{PBel} neurons (Figure S4J). Although the difference between ipsilateral and contralateral stimulation
202 was observed in CGRP^{SPFp} neurons, these neurons were robustly activated by thermal noxious stimuli from
203 both sides (Figures S4K–N). Interestingly, calcium responses induced by mechanical stimuli were much
204 higher than those induced by thermal stimuli in CGRP^{SPFp} neurons; the opposite was observed for CGRP^{PBel}
205 neurons. These results indicate that the CGRP^{SPFp} and CGRP^{PBel} neurons may play different roles in
206 conveying mechanical and thermal pain.

207 To assess the effects of inflammatory pain, we injected 10 μ l of 4% formalin into the contralateral
208 forepaw, and calcium activity was recorded with fiber photometry under light anesthesia (Figures 2P-U).
209 We observed increases in activity during both the initial acute pain phase (5–10 min; Figures 2Q, and T)
210 and the inflammatory phase (15–45 min; Figures 2R, and U). Activation of these neurons by formalin was
211 confirmed by Fos immunostaining, which again showed that bilateral CGRP^{SPFp} and CGRP^{PBel} neurons
212 were activated by unilateral stimuli with greater response in the contralateral neurons (Figures S5A-G).

213 Our data indicate that multimodal nociceptive stimuli bilaterally activate CGRP^{SPFp} and CGRP^{PBel}
214 neurons and that these two populations differentially respond to nociceptive inputs of distinct modalities.
215 Moreover, there is evidence for a potential inhibitory circuit to CGRP^{PBel} neurons, as we found activity
216 decreases in response to 300 g of mechanical pain and during the acute phase of the formalin test.

217

218 **Pain-induced synaptic plasticity change in CGRP^{SPFp} and CGRP^{PBel} neurons**

219 As we observed that noxious stimuli activate CGRP^{SPFp} and CGRP^{PBel} neurons, we hypothesized that pain
220 may alter the glutamatergic synaptic strength of these neurons. We performed *ex vivo* electrophysiology to
221 tested pain-induced synaptic plasticity changes. To induce pain, we injected 50 μ l of 5% formalin into the
222 upper lip. Twenty-four hours after the injection, we prepared acute brain slices that contained the SPFp
223 (Figure 3A) or PBel (Figure 3I). We then measured the AMPA/NMDA ratio, an index of glutamatergic
224 synaptic strength, for both CGRP^{SPFp} and CGRP^{PBel} neurons using the whole-cell patch clamp recording.
225 For both CGRP^{SPFp} (Figures 3B, and C) and CGRP^{PBel} neurons (Figures 3J, and K), the AMPA/NMDA
226 ratio increased (indicating long-term potentiation) in mice treated with formalin compared to controls. No
227 differences were observed in the paired-pulse ratio (which indicates a presynaptic mechanism) for
228 CGRP^{SPFp} neurons (Figures 3D, and E), but an increase in this ratio was found for CGRP^{PBel} neurons
229 (Figures 3L, and M). To determine whether the AMPA current was affected, we recorded AMPA-mediated
230 mini EPSCs (Figures 3F, and N). mEPSC amplitude (Figure 3G), but not frequency (Figure 3H), increased
231 in CGRP^{SPFp} neurons of mice subjected to pain compared with controls. For CGRP^{PBel} neurons, the pain did
232 not affect mEPSC amplitude (Figure 3O) but decreased frequency (Figure 3P).

233 These data together suggest that CGRP^{SPFp} and CGRP^{PBel} neuronal synapses increase the strength of
234 glutamatergic signaling in response to pain.

235

236 **The transcriptome profiling of CGRP^{SPFp} and CGRP^{PBel} neurons**

237 To further investigate whether CGRP^{SPFp} and CGRP^{PBel} neurons exhibit specific transcriptomic profiles
238 associated with the affective pain perception, we conducted cell-type-specific transcriptomic profiling of
239 CGRP neurons in the SPFp and PBel regions. The *Calca*^{CreER} mouse line was crossed with the RiboTag
240 mouse line (Sanz et al., 2009) that has a floxed allele of hemagglutinin (HA)-tagged *Rpl22* gene. As a
241 result, the HA-tagged ribosomal protein, RPL22 is Cre-dependently expressed in the CGRP-expressing
242 neurons. After fresh brain tissues containing the SPFp or PBel region were collected and homogenized, the
243 ribosome-associated transcriptome was captured by immunoprecipitation with anti-HA antibody-
244 conjugated magnetic beads. Precipitated / unprecipitated total RNAs were sequenced to profile active
245 transcriptome enriched / deenriched in CGRP^{SPFp} and CGRP^{PBel} neurons. RNA sequencing results revealed
246 that the *Calca* gene that encodes CGRP is highly enriched in both CGRP^{SPFp} and CGRP^{PBel}-specific
247 transcriptome, which served as a positive control. Moreover, genes encoding neuropeptide were specifically
248 enriched in CGRP^{PBel} neurons (Figure 4D), and genes encoding markers for inhibitory neurons or glia were
249 de-enriched in both regions (Figure 4E), confirming that these neurons are glutamatergic neurons. Notably,
250 several pain-related genes, in particular those encoding membrane proteins, were enriched in both
251 populations (Figures 4A-C). Interestingly, genes associated with affective pain disorders, such as *Scn9a*,
252 and *Faah* for congenital insensitivity to pain (CIP), and *Cacna1a* for migraine (Nassar et al., 2004; van den
253 Maagdenberg et al., 2004; Cravatt and Lichtman, 2004) are highly enriched in these neurons (Figures 4A-
254 C). Expression of the proteins encoded by these genes (Nav1.7, Cav2.1, and FAAH) in the SPFp and PBel
255 was confirmed via immunohistochemistry (Figures 4F-H). These data indicate that both CGRP^{SPFp} and

256 CGRP^{PBel} neurons express genes involved in pain perception, further supporting our results that these
257 neurons form ascending pain pathways.

258

259 **CGRP^{SPFp} and CGRP^{PBel} neurons are activated by multisensory innate threat stimuli**

260 Our retrograde tracing results indicate that both CGRP^{SPFp} and CGRP^{PBel} neurons receive inputs from areas
261 conveying sensory information from multiple sensory modalities. We, therefore, examined whether they
262 are also activated by multisensory innate threat stimuli. We used the fiber photometry system to measure
263 neural activity in response to five different aversive sensory stimuli. AAV-DIO-GCaMP7s was injected
264 into the SPFp or PBel of *Calca^{Cre}* mice, and an optic fiber (400 μ m, 0.37 NA) was implanted above the
265 injections site to measure calcium activity of CGRP^{SPFp} or CGRP^{PBel} neurons (Figures 5A, and B). A
266 somatosensory stimulus was first tested by applying a foot shock in a cued fear conditioning test (Figure
267 5C). We associated a non-aversive low-volume tone (70 dB) with the shock to minimize the tone's aversive
268 effect (Figure S6A). For both CGRP^{SPFp} and CGRP^{PBel} neurons, immediate increases in neural activity were
269 detected in response to the 2-s foot shock, but not during habituation or during the cue test (when the tone
270 was on; Figures 5D–E). Freezing was observed during the cue test, indicating that fear memory was formed
271 (Figures S6B, and C). To assess the auditory threat, an intense sound (85 dB) was delivered for 2 s (Figure
272 5F). Time-locked calcium responses were detected at the onset of an 85-dB intense sound, but not a 70-dB
273 sound for both CGRP^{SPFp} (Figure 5G) and CGRP^{PBel} neurons (Figure 5H). For an innate visual stimulus, a
274 2-s looming stimulus was given three times with 10-s intervals. Both CGRP^{SPFp} (Figure 5J) and CGRP^{PBel}
275 neurons (Figure 5K) displayed an increase of activity in response to the looming (large disk) compared to
276 the control (small disk) stimulus. As an innate olfactory stimulus test, we exposed mice to a cotton swap
277 soaked with trimethylthiazoline (TMT; Figure 5L). CGRP^{SPFp} neurons did not respond to TMT (Figure 5M),
278 whereas CGRP^{PBel} neurons exhibited a slight increase in activity (Figure 5N). Finally, a gustatory stimulus
279 was administered by exposing mice to quinine (vs. water; Figure 5O). When overnight water restricted mice
280 licked quinine solution (0.5 mM), CGRP^{SPFp} neurons did not respond, compared with water controls (Figure
281 5P), but CGRP^{PBel} neurons exhibited an increase in calcium activity (Figure 5Q). The calcium peak
282 amplitude analysis shows that the calcium responses between the CGRP^{SPFp} and CGRP^{PBel} neurons were
283 not significantly different by somatosensory and auditory stimuli (Figures S7A, and B). However, the
284 CGRP^{SPFp} neurons showed a greater response to the visual stimulus compared to the CGRP^{PBel} neurons
285 (Figure S7C). In contrast, the CGRP^{PBel} neurons showed greater responses to the olfactory and gustatory
286 stimuli compared to the CGRP^{SPFp} neurons (Figures S7D, and E).

287 Our results indicate that the CGRP^{SPFp} and CGRP^{PBel} neurons are both involved in the perception of
288 innate multisensory threat but respond differently to inputs from distinct modalities. CGRP^{PBel} neurons were
289 activated by all five aversive sensory stimuli, whereas the CGRP^{SPFp} neurons were only activated by
290 somatosensory, auditory, and visual aversive stimuli.

291

292 **Silencing CGRP neurons attenuates responses to multimodal threat stimuli**

293 Our rabies tracing and fiber photometry results imply that CGRP^{SPFp} and CGRP^{PBel} neurons are critically
294 involved in innate threat perception. Thus, we next tested whether these neurons are necessary for innate
295 threat perception. We silenced these neurons by bilateral injection of AAV-DIO-TetTox::GFP into the
296 SPFp or PBel of *Calca^{Cre}* mice and measured behavioral responses to pain stimuli, and multimodal aversive
297 threat stimuli (Figure 6A). We first performed the formalin assay to test the affective pain perception
298 (Figure 6B). Following injection of 4% formalin into the forepaw, mice in which CGRP^{SPFp} or CGRP^{PBel}
299 neurons were silenced spent less time licking the injected paw (Figure 6C). In addition, the CGRP^{SPFp}

300 silenced group exhibited decreased thermal sensitivity in the 55 °C hot plate test (Figure S8A, B), decreased
301 mechanical sensitivity in the electronic von Frey test (Figures S8C, and D), and decreased freezing in
302 response to the contextual fear conditioning test (Figures S8E, and F). Interestingly, previous results with
303 CGRP^{PBeI}-silenced mice by TetTox exhibited no changes in thermal or mechanical thresholds but decreased
304 freezing in the fear conditioning test (Han et al., 2015), suggesting that both CGRP^{SPFp} and CGRP^{PBeI}
305 neurons are necessary for affective pain perception. However, CGRP^{SPFp} neurons, not CGRP^{PBeI} neurons,
306 are also necessary for sensory pain perception. The elevated plus maze (EPM) test shows that silencing the
307 CGRP^{SPFp} or CGRP^{PBeI} neurons decreased anxiety-like behaviors in mice (Figures S8G, and H).

308 To test the role of these neurons on multisensory threat perception, these mice were subjected to the
309 multiple aversive sensory threat cues, as described in Figure 5. Levels of immediate freezing in response to
310 the aversive somatosensory stimulus (2-s, 0.6 mA electric foot shock) were significantly reduced in both
311 the CGRP^{SPFp} and CGRP^{PBeI} TetTox groups compared to the EYFP control groups (Figure 6D). In the
312 auditory threat test with 85-dB intense sound, EYFP control mice displayed freezing behavior, but freezing
313 levels were reduced in both the CGRP^{SPFp} and CGRP^{PBeI} TetTox groups (Figure 6E). Defensive behaviors
314 (freezing) were also attenuated in response to a looming visual stimulus in the CGRP^{SPFp} TetTox group
315 compared with controls, but no difference in freezing was observed between the CGRP^{PBeI} TetTox group
316 and controls (Figure 6F). Interestingly, CGRP^{PBeI} neurons were activated by looming (Figure 5K), but their
317 silencing was not enough to attenuate the animal's response to a visual threat, indicating that they play a
318 less significant role in transmitting aversive visual stimulus to the amygdala compared to the CGRP^{SPFp}
319 neurons. The aversive olfactory test was performed using a two-chamber system, with one chamber
320 containing water-soaked cotton and the other containing TMT-soaked cotton. Silencing the CGRP^{SPFp}
321 neurons did not affect the perception of aversive olfactory cue, as these mice and EYFP controls both
322 avoided the TMT chamber, while the CGRP^{PBeI} TetTox group exhibited no aversion to TMT, spending
323 equal amounts of time in the water and TMT chambers (Figure 6G). The gustatory test was performed as a
324 two-bottle choice test between water and quinine solution. The CGRP^{SPFp} TetTox consumed minimal
325 quinine solution (0.5 mM), like controls, whereas the CGRP^{PBeI} TetTox group showed much less aversion
326 to quinine (Figure 6H).

327 These results indicate that both the CGRP^{SPFp} and CGRP^{PBeI} neurons are necessary for the perception of
328 innate sensory threat cues, as well as affective pain.

329

330 **Activating CGRP^{SPFp}/CGRP^{PBeI} to amygdala pathways induces negative valence**

331 Next, we performed optogenetic gain-of-function experiments to test whether activation of these neurons
332 is sufficient to induce negative affect in mice. We bilaterally injected AAV-DIO-ChR2 into the SPFp of
333 *Calca^{Cre}* mice and implanted optic fibers (200 μm, NA 0.22) above the injection site (Figure 7A). 20-Hz
334 photo-stimulation of CGRP^{SPFp} neurons did not change responses in the hot plate thermal sensitivity test
335 and the electronic von Frey mechanical threshold test for sensory and discriminative pain perception
336 (Figures S8I-L). To test whether these neurons encode negative valence, we performed the real-time place
337 aversion (RTPA) test. Optogenetic stimulation is delivered only when the test mouse stays on one side of a
338 two-chamber apparatus (Stamatakis and Stuber, 2012; Figure 7B). Optogenetic activation of the CGRP^{SPFp}
339 neurons induced aversion to the photo-stimulated chamber, suggesting that these neurons play a role in
340 negative emotion or affective-motivational pain (Figures 7B, and C). Next, we replaced the foot shock with
341 photo-stimulation (20 Hz) as the unconditioned stimulus (US) in the context and cued fear conditioning
342 test. This was to assess whether activation of CGRP^{SPFp} neurons was sufficient to induce fear behaviors.
343 Context-dependent optogenetic conditioning was achieved by 10 mins of photo-stimulation in an open field

344 arena; freezing behavior was then assessed in the same context 24 h after the conditioning (Figure S8M).
345 The Chr2 group exhibited more freezing than the control group, suggesting that CGRP^{SPFp} activation can
346 act as the US (Figure S8N). For cue-dependent optogenetic conditioning, photo-stimulation was associated
347 with a tone as a non-noxious conditioned stimulus (CS+) in a fear conditioning chamber (Figure S8O). Both
348 context and cue tests were performed after the conditioning. The Chr2 group exhibited more freezing in
349 both context (Figure S8P) and cue tests (Figure S8Q). Together with the optogenetic conditioning results
350 of CGRP^{PBel} neurons in the previous result (Han et al., 2015), these results indicate that activation of both
351 CGRP^{SPFp} and CGRP^{PBel} neurons is sufficient to induce negative valence associated with affective-
352 motivational pain perception.

353 We then sought to characterize the functional downstream of the CGRP^{SPFp} neurons. To examine the
354 functional connectivity of anatomical downstream regions from the CGRP^{SPFp} neurons, we performed *ex*
355 *vivo* electrophysiology recording. AAV-DIO-ChR2-EYFP was injected into the SPFp of *Calca*^{Cre} mice
356 (Figure S9A). After four weeks of Chr2 expression, we performed whole-cell recordings of neurons from
357 AStr, LA, and pIC to measure optogenetically-evoked excitatory/inhibitory postsynaptic currents
358 (EPSC/IPSC) (Figure S9B). We found that CGRP^{SPFp} neurons form functional glutamatergic synapses with
359 neurons within AStr, LA (Figure S9C), and pIC (data not shown). Moreover, the onset of IPSCs lagged 4–
360 5 ms compared to the onset of EPSCs, indicating a feed-forward inhibition circuit. The number of cells that
361 had both EPSCs and IPSCs, EPSCs only, IPSCs only, and non-responsive were also counted (Figures S9D-
362 L). To investigate whether these connections form functional circuits that encode negative valence, we
363 optogenetically stimulated axonal terminals from the CGRP^{SPFp} neurons and performed behavioral tests.
364 AAV-DIO-ChR2-EYFP was injected into the SPFp of the *Calca*^{Cre} mice, and optical fibers were implanted
365 into the postsynaptic areas of CGRP^{SPFp} neurons, namely the LA, AStr, and pIC (Figure 7D). Optogenetic
366 activation of each of these three projections induced aversion in the RTPA experiment (Figures 7E, and
367 S9M), as observed in direct photo-stimulation of CGRP^{SPFp} cell bodies (Figure 7C). Cue-dependent
368 optogenetic conditioning of the downstream circuits was then performed and only the CGRP^{SPFp}→LA circuit
369 caused significant freezing in the context test (Figure 7F). The other two projections only showed a trend
370 (Figure S9N). Increased freezing was observed in the cue test for all three projections (Figures 7G, and
371 S9O), but the most prominent effect was observed with the CGRP^{SPFp}→LA circuit.

372 The same behavioral experiments were performed as above with the CGRP^{PBel} neurons to compare their
373 role in encoding negative valence with the CGRP^{SPFp} neurons. First, photo-stimulation of the CGRP^{PBel}
374 neuronal cell body (Figure 7H) induced aversion during the RTPA test (Figures 7I, and J). Then, we
375 investigated the CGRP^{PBel}→CeA circuit as in Figure 7D-H by optogenetic terminal stimulation (Figure 7K).
376 Photo-stimulation of CGRP^{PBel}→CeA terminals induced aversion in the RTPA test (Figure 7L), and freezing
377 in the optogenetic conditioning context, and cue tests (Figures 7M, and N).

378 These results satisfy the idea that CGRP^{SPFp}→LA and CGRP^{PBel}→CeA circuits induce negative valence either
379 by affective pain or innate sensory threat cues.

380 **Discussion**

381 We report that a genetically defined population of neurons that express the neuropeptide CGRP in the SPFP
382 and PBel mediate perception of not only affective pain but also innate sensory threat cues. They perform
383 this function by relaying aversive sensory signals from the spinal cord and all other sensory relay areas to
384 the amygdala. These analyses provide the first evidence of convergent multisensory threat pathways that
385 relays all aversive sensory modalities to the amygdala.

387 **Encoding affective pain signals to the amygdala**

388 Perception of pain protects us from physical harm by locating the source of a harmful stimulus. Painful
389 experiences also elicit emotional and motivational responses, which help us remember these events and
390 avoid similar stimuli in the future (Yeh et al., 2018). Thus, pain is not just a simple sensory process but also
391 a complex cognitive process that generates sensory and emotional responses. This unique aspect of pain
392 gives rise to the concept of two aspects of pain: sensory-discriminative and affective-motivational (Auvray
393 et al., 2010; Melzack and Casey, 1968). It is thought that the sensory-discriminative aspect of pain is
394 processed within the sensory cortex via the spino-thalamic tract, and the affective-motivational aspect of
395 pain is processed within the amygdala via the spino-parabrachial tract. Indeed, previous studies have shown
396 that the PBN-to-CeA circuit is critical for affective-motivational pain perception (Han et al., 2015; Sato et
397 al., 2015). However, it has also been suggested that the thalamus is actively involved in affective-
398 motivational pain perception (Craig, 2003; Willis et al., 2002). Previous tracing studies have confirmed that
399 projection neurons from the superficial dorsal horn of the spinal cord relay pain signals directly to various
400 brain areas, including the thalamus. Importantly, posterior regions of the thalamus (e.g., the VMpo in
401 primates and humans, as well as the SPFP and PoT in rodents) are anatomically connected to limbic areas
402 (Craig, 1998; Gauriau and Bernard, 2004a) and activated by noxious stimuli (Craig et al., 1994; Peschanski
403 et al., 1981). Therefore, the thalamus likely also plays a critical role in affective-motivational aspects of
404 pain perception by relaying noxious information to limbic areas such as the amygdala. Our results
405 demonstrate that a genetically defined population of neurons within the SPFP of the thalamus express the
406 neuropeptide CGRP and receive monosynaptic inputs from projection neurons within the spinal dorsal horn.
407 They then project to specific nuclei within the amygdala, namely the AStr and LA (Figure 1). Multimodal
408 nociceptive stimuli activate these neurons in an intensity-dependent manner in anesthetized mice (Figure
409 2). Inactivating these neurons attenuates the perception of affective-motivational pain, and pain signals
410 increase the synaptic plasticity of these neurons (Figure 3). These data indicate that CGRP^{SPFP} neurons form
411 the spino-thalamo-amygdaloid affective pain pathway.

412
413 Unlike the STT, the SPT has been well-characterized as an affective-motivational pain pathway. Recent
414 studies have shown that the lateral PBN receives direct nociceptive inputs from projection neurons within
415 the spinal dorsal horn (Barik et al., 2020; Chiang et al., 2020; Choi et al., 2020; Deng et al., 2020). The
416 dorsolateral PBN (PBdl) receives predominantly nociceptive inputs from the spinal cord and then projects
417 to multiple limbic structures, such as the PAG, VMH, and ILN, thereby producing emotional and
418 physiological changes in response to pain signals (Chiang et al., 2020; Deng et al., 2020). Although the
419 PBdl does not directly project to the amygdala, it indirectly sends pain signals to the CeA through the PBel
420 (Deng et al., 2020). In particular, CGRP^{PBel} neurons are critical for relaying aversive unconditioned stimuli
421 to the CeA during aversive fear learning (Han et al., 2015). It has been shown that these neurons receive
422 direct inputs from dynorphin neurons in the PBdl (Chiang et al., 2020), and a recent study has shown that
423 spinal projection neurons that express GPR83 directly innervate CGRP^{PBel} neurons to relay noxious signals

424 (Choi et al., 2020). Therefore, it is clear that CGRP^{PBeI} neurons relay nociceptive information from the PBdl
425 and the spinal cord to the CeA. Our results show that CGRP^{PBeI} neurons receive direct synaptic inputs from
426 the spinal cord (Figure 1), exhibit intensity-dependent activation by multimodal nociceptive stimuli in
427 anesthetized mice (Figure 2), and exhibit increased synaptic plasticity in the context of pain signals (Figure
428 3). Therefore, together with previous studies, our results reaffirm that CGRP^{PBeI} neurons comprise the
429 spino-parabrachio-amygdaloid pain pathway.

430
431 Monitoring calcium activity of the CGRP^{SPFp} and CGRP^{PBeI} neurons in response to multimodal nociceptive
432 stimuli at various intensities in anesthetized mice provides us novel insights into understanding central
433 affective pain pathways. First, unlike sensory pain signals are conveyed to the contralateral side of the
434 somatosensory cortex, these neurons are activated by both contralateral and ipsilateral noxious stimulation
435 indicating that the affective pain pathway may not be strictly lateralized (Figure S4). Second, the CGRP^{SPFp}
436 neurons more robustly respond to the mechanical stimulus, whereas the CGRP^{PBeI} neurons respond more
437 robustly to the thermal stimulus suggesting that these two parallel pathways may convey different modality
438 of nociceptive information (Figure 2). Lastly, the CGRP^{PBeI} neurons are activated at lower stimulus intensity
439 but respond slowly compared to the CGRP^{SPFp} neurons (Figures 2, S4). Therefore, our results demonstrate
440 that CGRP-expressing neurons in two brain areas (the SPFp and PBeI) play complementary roles in relaying
441 multimodal nociceptive signals from the spinal cord to the amygdala through two parallel ascending pain
442 pathways, which is critical for affective-motivational pain perception.

443
444 **Encoding multimodal threat cues to the amygdala**

445 Both pain and innate sensory threats motivate animals to execute immediate avoidance behaviors to escape
446 the threatening or tissue-damaging situation, and produce long-lasting aversive memories. Indeed,
447 Pavlovian threat conditioning uses noxious electric foot shock, an acute painful stimulus that motivates the
448 animals to create aversive memory (LeDoux, 2012; Maren, 2001). However, the neural circuit mechanisms
449 by which noxious information is conveyed to the amygdala during aversive learning is not fully understood.
450 Recent advances in the neural circuit-based understanding of innate predator threat perception suggest that
451 innate threat cues from each sensory modality are conveyed through separate neural pathways (Canteras,
452 2002; Gross and Canteras, 2012; Kunwar et al., 2015; Silva et al., 2013), which do not overlap with the
453 unconditioned stimulus (affective pain) pathway in Pavlovian threat learning (Silva et al., 2016). However,
454 it is logical to think that the integration of threat stimuli conveyed by different sensory modalities is crucial
455 for perceiving a threat because animals use multiple senses simultaneously to search for and detect
456 imminent threats. Moreover, previous clinical studies have shown that pain and threat perceptions interact
457 with each other (Berthier et al., 1988; Elman and Borsook, 2018). Therefore, it is plausible that there is a
458 unified mechanism that conveys all aversive sensory information to the amygdala. Our results demonstrate
459 that CGRP-expressing neurons in the PBeI and the SPFp not only relay nociceptive stimuli to the amygdala
460 during aversive learning, but they also convey innate sensory threat cues from all sensory modalities
461 (Figures 5, 6). The CGRP^{SPFp} neurons relay aversive sensory cues from the somatosensory, visual, and
462 auditory modalities to the LA, AStr, and pIC. By contrast, CGRP^{PBeI} neurons relay aversive cues from all
463 sensory modalities (somatosensory, visual, auditory, olfactory, and gustatory) (Figures 5, 6, and S3). In
464 addition, previous studies have shown that CGRP^{PBeI} neurons are activated by hypercapnic conditions (high
465 CO₂ levels) (Kaur et al., 2017; Yokota et al., 2015), and aversive visceral cues, such as lithium chloride and
466 lipopolysaccharide (Carter et al., 2013; Paues et al., 2001). Therefore, it is tempting to speculate that

467 CGRP^{SPFp} neurons relay exteroceptive threat signals, whereas CGRP^{PBel} neurons relay both exteroceptive
468 and interoceptive threat signals to the amygdala.

469

470 In consistency with a previous report (Han et al., 2015), our data provide strong evidence that the CGRP^{PBel}
471 neurons mediate aversive learning via their projection to the CeA (Figure 7K-N). This seems to be
472 contradictory to a recent study by Bowen et al., (2020), which argued that optogenetic stimulation of
473 CGRP^{PBel} axon terminals in the parvocellular portion of the ventroposteromedial nucleus of the thalamus
474 (VPMpc), instead of the CeA, evokes strong aversive memory. This discrepancy can be explained by the
475 differences in optogenetic stimulation protocols. Whereas we used a 40 Hz light stimulation for 10 s as
476 described (Han et al., 2015), Bowen et al. used a 30 Hz light train for only 2 s. Moreover, it is worth noting
477 that axonal bundles from all glutamatergic neurons in the PBel that project to forebrain regions, including
478 the CeA, BNST, and PSTN pass through the VPMpc (Huang et al., 2020), which suggests that optogenetic
479 stimulation within the VPMpc activates both CGRP^{PBel} axonal terminals and axon bundles passing through
480 this area. Therefore, an alternative explanation of their observation is that concurrent stimulation of all
481 downstream areas produces stronger aversive memory than stimulating CeA alone.

482

483 **Pain-threat interactions in affective pain disorders**

484 Our results show that the affective-motivational pain and multisensory threat stimuli arrive in the amygdala
485 via the same neural pathways. Interestingly, pain-threat interactions have been reported in many human
486 clinical cases. People with pain asymbolia, caused by damage to limbic areas of the brain, have the normal
487 sensory perception of noxious stimuli, but they have impaired affective pain perception (Berthier et al.,
488 1988). Interestingly, pain asymbolia patients often display deficits in perceiving general threats (Klein,
489 2015; Price, 2000), indicating that the perception of affective pain and other sensory threat cues share the
490 same neural substrate. People with congenital insensitivity to pain (CIP) are insensitive to all sensory and
491 affective components of pain, but they also display profound deficits in general threat perception, which is
492 the primary cause of their short life expectancy (McMurray, 1955; Nagasako et al., 2003). CIP is caused by
493 loss-of-function mutations in genes critical for pain transmission, such as *Scn9a* (Dabby, 2012; Fischer and
494 Waxman, 2010; Lampert et al., 2010) and *Faah* (Drissi et al., 2020). *Scn9a* encodes voltage-gated sodium
495 channel type 7 (Nav1.7), and *Faah* encodes fatty acid amide hydrolase, both of which are critical for pain
496 transmission in the spinal cord (Cajanus et al., 2016; Kim et al., 2006; Nantermet and Henze, 2011; Nassar
497 et al., 2004). However, functional loss of these genes in the spinal neurons cannot explain the insensitivity
498 to general threats exhibited by CIP patients. Surprisingly, our cell type-specific transcriptome analysis
499 revealed that *Scn9a* and *Faah* transcripts are highly enriched in both CGRP^{PBel} and CGRP^{SPFp} neurons
500 (Figure 4). Thus, mutations in these genes may prevent these neurons from relaying sensory threat signals
501 to the amygdala, thereby causing insensitivity to general threats in CIP. This speculation should be
502 addressed by testing the causal relationship between mutations in these genes in CGRP neurons and threat
503 perception.

504

505 Opposite clinical cases also exist. People with affective pain disorders, such as migraine, and fibromyalgia
506 experience chronic pain and suffer from hypersensitivity to normal sensory stimuli (Demarquay and
507 Mauguière, 2016; Harriott and Schwedt, 2014; Harte et al., 2016; López-Solà et al., 2017). Further, normal
508 sensory stimuli often trigger or aggravate their pain symptoms (Bar-Shalita and Cermak, 2020; Bar-Shalita
509 et al., 2019). Surprisingly, the gene *Cacna1a*, which has been linked to migraines, is highly enriched in
510 both CGRP^{PBel} and CGRP^{SPFp} neurons (Figure 4). Further studies should address the causal relationship

511 between loss of *Cacna1a* function in CGRP neurons and sensory hypersensitivity in migraine. In addition,
512 CGRP signaling is a proven therapeutic target for treating migraine (Ashina, 2020). Therefore, we speculate
513 that the CGRP-expressing neurons characterized in this study may serve as the functional substrate for
514 sensory hypersensitivity in migraine. We also speculate that CGRP receptor antagonists or neutralizing
515 monoclonal antibodies used to treat migraine may serve as potential therapeutic interventions for treating
516 threat-related disorders, such as phobias, panic disorder, and post-traumatic stress disorder.

517

518 **Conclusion**

519 Our findings demonstrate that CGRP^{SPFP} neurons form a novel spino-thalamo-amygdaloid affective pain
520 pathway and, together with the previously characterized CGRP^{PBeI} neurons, serve as complementary
521 parallel pathways for conveying the unconditioned stimulus during Pavlovian threat learning. Furthermore,
522 our analyses reveal that these parallel unconditioned stimulus pathways not only relay pain signals to the
523 amygdala but also convey aversive sensory cues from all sensory modalities to the amygdala (Figure S10).
524 The discovery of a unified threat perception system for transmitting multimodal interoceptive and
525 exteroceptive aversive sensory stimuli greatly enhances our understanding of the neural mechanisms of
526 innate threat perception. These insights also provide novel targets for developing therapeutic interventions
527 against affective pain and innate fear-related disorders.

528

529 **Acknowledgments**

530 We thank Dr. D. O'Keefe, Ms. C. Jia, and Han lab members for critical discussions during manuscript
531 preparation. S.H. is supported by 1R01MH116203 from NIMH and the Bridge to Independence award from
532 the Simons Foundation Autism Research Initiative (SFARI #388708). S.L. is supported by the Salk Women
533 & Science Special Award, the Mary K. Chapman Foundation, and the Jesse & Caryl Philips Foundation.

534

535

536

537 **Author Contributions**

538 S.H. conceived of the idea and secured funding. S.H., S.J.K., S.L., and M.Y. designed the experiments and
539 wrote the manuscript. S.J.K. performed most of the CGRP^{SPFp} experiments. S.L., and S.J.K. performed
540 CGRP^{PBel} experiments. M.Y. performed electrophysiology and CGRP^{PBel} RTPA. D.I.K., and J.H.K.
541 performed RiboTag experiments, and T.G.O analyzed it. R.M.E. provided resources for Ribotag analysis.
542 J.P. performed spinal projection histology experiments. M.G. provided *Cdx2^{FlpO}* mouse line. K.F.L.
543 provided resources for microscopy.

544

545 **Declaration of Interests**

546 The authors declare no competing interests.

547

548 **References**

- 549 Al-Khater, K.M., Kerr, R., and Todd, A.J. (2008). A quantitative study of spinothalamic neurons in laminae
550 I, III, and IV in lumbar and cervical segments of the rat spinal cord. *J. Comp. Neurol.* *511*, 1–18.
- 551 Ashina, M. (2020). Migraine. *N. Engl. J. Med.* *383*, 1866–1876.
- 552 Auvray, M., Myin, E., and Spence, C. (2010). The sensory-discriminative and affective-motivational
553 aspects of pain. *Neurosci. Biobehav. Rev.* *34*, 214–223.
- 554 Bach, D.R., Hurlmann, R., and Dolan, R.J. (2015). Impaired threat prioritisation after selective bilateral
555 amygdala lesions. *Cortex* *63*, 206–213.
- 556 Barik, A., Sathyamurthy, A., Thompson, J., Seltzer, M., Levine, A., and Chesler, A. (2020). A
557 spinoparabrachial circuit defined by *Tacr1* expression drives pain. *BioRxiv* 2020.07.15.205484.
- 558 Bar-Shalita, T., and Cermak, S.A. (2020). Multisensory Responsiveness and Personality Traits Predict
559 Daily Pain Sensitivity. *Front. Integr. Neurosci.* *13*, 77.
- 560 Bar-Shalita, T., Granovsky, Y., Parush, S., and Weissman-Fogel, I. (2019). Sensory Modulation Disorder
561 (SMD) and Pain: A New Perspective. *Front. Integr. Neurosci.* *13*.
- 562 Barsy, B., Kocsis, K., Magyar, A., Babiczky, Á., Szabó, M., Veres, J.M., Hillier, D., Ulbert, I., Yizhar, O., and
563 Mátyás, F. (2020). Associative and plastic thalamic signaling to the lateral amygdala controls fear
564 behavior. *Nat. Neurosci.* *23*, 625–637.
- 565 Basbaum, A.I., Bautista, D.M., Scherrer, G., and Julius, D. (2009). Cellular and Molecular Mechanisms of
566 Pain. *Cell* *139*, 267–284.
- 567 Bernard, J.F., Huang, G.F., and Besson, J.M. (1992). Nucleus centralis of the amygdala and the globus
568 pallidus ventralis: electrophysiological evidence for an involvement in pain processes. *J. Neurophysiol.*
569 *68*, 551–569.
- 570 Berthier, M., Starkstein, S., and Leiguarda, R. (1988). Asymbolia for pain: A sensory-limbic disconnection
571 syndrome. *Ann. Neurol.* *24*, 41–49.
- 572 Bester, H., Matsumoto, N., Besson, J.M., and Bernard, J.F. (1997). Further evidence for the involvement
573 of the spinoparabrachial pathway in nociceptive processes: a c-Fos study in the rat. *J. Comp. Neurol.*
574 *383*, 439–458.
- 575 Blanchard, D.C., and Blanchard, R.J. (1972). Innate and conditioned reactions to threat in rats with
576 amygdaloid lesions. *J. Comp. Physiol. Psychol.* *81*, 281–290.
- 577 Bourane, S., Grossmann, K.S., Britz, O., Dalet, A., Del Barrio, M.G., Stam, F.J., Garcia-Campmany, L., Koch,
578 S., and Goulding, M. (2015). Identification of a Spinal Circuit for Light Touch and Fine Motor Control. *Cell*
579 *160*, 503–515.
- 580 Bowen, A.J., Chen, J.Y., Huang, Y.W., Baertsch, N.A., Park, S., and Palmiter, R.D. (2020). Dissociable
581 control of unconditioned responses and associative fear learning by parabrachial CGRP neurons. *ELife* *9*,
582 e59799.

- 583 Bushnell, M.C., Čeko, M., and Low, L.A. (2013). Cognitive and emotional control of pain and its
584 disruption in chronic pain. *Nat. Rev. Neurosci.* *14*, 502–511.
- 585 Cajanus, K., Holmström, E.J., Wessman, M., Anttila, V., Kaunisto, M.A., and Kalso, E. (2016). Effect of
586 endocannabinoid degradation on pain: role of FAAH: polymorphisms in experimental and postoperative
587 pain in women treated for breast cancer. *PAIN* *157*, 361–369.
- 588 Canteras, N.S. (2002). The medial hypothalamic defensive system: Hodological organization and
589 functional implications. *Pharmacol. Biochem. Behav.* *71*, 481–491.
- 590 Carter, M.E., Soden, M.E., Zweifel, L.S., and Palmiter, R.D. (2013). Genetic identification of a neural
591 circuit that suppresses appetite. *Nature advance online publication*.
- 592 Chapman, C.R., and Nakamura, Y. (1999). A Passion of the Soul: An Introduction to Pain for
593 Consciousness Researchers. *Conscious. Cogn.* *8*, 391–422.
- 594 Chen, J.Y., Campos, C.A., Jarvie, B.C., and Palmiter, R.D. (2018). Parabrachial CGRP Neurons Establish and
595 Sustain Aversive Taste Memories. *Neuron* *100*, 891-899.e5.
- 596 Chiang, M.C., Nguyen, E.K., Canto-Bustos, M., Papale, A.E., Oswald, A.-M.M., and Ross, S.E. (2020).
597 Divergent Neural Pathways Emanating from the Lateral Parabrachial Nucleus Mediate Distinct
598 Components of the Pain Response. *Neuron* *106*, 927-939.e5.
- 599 Choi, S., Hachisuka, J., and Ginty, D. (2020). Parallel ascending spinal pathways for affective touch and
600 pain. *Nature In press*.
- 601 Coolen, L.M., Veening, J.G., Wells, A.B., and Shipley, M.T. (2003a). Afferent connections of the
602 parvocellular subparafascicular thalamic nucleus in the rat: Evidence for functional subdivisions. *J.*
603 *Comp. Neurol.* *463*, 132–156.
- 604 Coolen, L.M., Veening, J.G., Petersen, D.W., and Shipley, M.T. (2003b). Parvocellular subparafascicular
605 thalamic nucleus in the rat: Anatomical and functional compartmentalization. *J. Comp. Neurol.* *463*,
606 117–131.
- 607 Corder, G., Ahanonu, B., Grewe, B.F., Wang, D., Schnitzer, M.J., and Scherrer, G. (2019). An amygdalar
608 neural ensemble that encodes the unpleasantness of pain. *Science* *363*, 276–281.
- 609 Craig, A.D. (1998). A new version of the thalamic disinhibition hypothesis of central pain. *Pain Forum* *7*,
610 1–14.
- 611 Craig, A.D. (Bud) (2003). PAIN MECHANISMS: Labeled Lines Versus Convergence in Central Processing.
612 *Annu. Rev. Neurosci.* *26*, 1–30.
- 613 Craig, A.D., Bushnell, M.C., Zhang, E.-T., and Blomqvist, A. (1994). A thalamic nucleus specific for pain
614 and temperature sensation. *Nature* *372*, 770–773.
- 615 Craig, A.D., Chen, K., Bandy, D., and Reiman, E.M. (2000). Thermosensory activation of insular cortex.
616 *Nat. Neurosci.* *3*, 184–190.

- 617 Cravatt, B.F., and Lichtman, A.H. (2004). The endogenous cannabinoid system and its role in nociceptive
618 behavior. *J. Neurobiol.* *61*, 149–160.
- 619 Dabby, R. (2012). Pain Disorders and Erythromelalgia Caused by Voltage-Gated Sodium Channel
620 Mutations. *Curr. Neurol. Neurosci. Rep.* *12*, 76–83.
- 621 Dado, R.J., Katter, J.T., and Giesler, G.J. (1994). Spinothalamic and spinothalamic tract neurons in
622 the cervical enlargement of rats. II. Responses to innocuous and noxious mechanical and thermal
623 stimuli. *J. Neurophysiol.* *71*, 981–1002.
- 624 Dal Monte, O., Costa, V.D., Noble, P.L., Murray, E.A., and Averbeck, B.B. (2015). Amygdala lesions in
625 rhesus macaques decrease attention to threat. *Nat. Commun.* *6*, 10161.
- 626 Demarquay, G., and Mauguière, F. (2016). Central Nervous System Underpinnings of Sensory
627 Hypersensitivity in Migraine: Insights from Neuroimaging and Electrophysiological Studies. *Headache J.*
628 *Head Face Pain* *56*, 1418–1438.
- 629 Deng, J., Zhou, H., Lin, J.-K., Shen, Z.-X., Chen, W.-Z., Wang, L.-H., Li, Q., Mu, D., Wei, Y.-C., Xu, X.-H., et al.
630 (2020). The Parabrachial Nucleus Directly Channels Spinal Nociceptive Signals to the Intralaminar
631 Thalamic Nuclei, but Not the Amygdala. *Neuron* *107*, 923.
- 632 D’Hanis, W., Linke, R., and Yilmazer-Hanke, D. m. (2007). Topography of thalamic and parabrachial
633 calcitonin gene-related peptide (CGRP) immunoreactive neurons projecting to subnuclei of the
634 amygdala and extended amygdala. *J. Comp. Neurol.* *505*, 268–291.
- 635 Dobolyi, A., Irwin, S., Makara, G., Usdin, T.B., and Palkovits, M. (2005). Calcitonin gene-related peptide-
636 containing pathways in the rat forebrain. *J. Comp. Neurol.* *489*, 92–119.
- 637 Drissi, I., Woods, W.A., and Woods, C.G. (2020). Understanding the genetic basis of congenital
638 insensitivity to pain. *Br. Med. Bull.* *133*, 65–78.
- 639 Elman, I., and Borsook, D. (2018). Threat Response System: Parallel Brain Processes in Pain vis-à-vis Fear
640 and Anxiety. *Front. Psychiatry* *9*.
- 641 Fischer, T.Z., and Waxman, S.G. (2010). Familial pain syndromes from mutations of the Nav1.7 sodium
642 channel. *Ann. N. Y. Acad. Sci.* *1184*, 196–207.
- 643 Gao, Y.-J., Ren, W.-H., Zhang, Y.-Q., and Zhao, Z.-Q. (2004). Contributions of the anterior cingulate cortex
644 and amygdala to pain- and fear-conditioned place avoidance in rats: *Pain* *110*, 343–353.
- 645 Gauriau, C., and Bernard, J.-F. (2002). Pain pathways and parabrachial circuits in the rat. *Exp. Physiol.* *87*,
646 251–258.
- 647 Gauriau, C., and Bernard, J.-F. (2004a). Posterior Triangular Thalamic Neurons Convey Nociceptive
648 Messages to the Secondary Somatosensory and Insular Cortices in the Rat. *J. Neurosci.* *24*, 752–761.
- 649 Gauriau, C., and Bernard, J.-F. (2004b). A comparative reappraisal of projections from the superficial
650 laminae of the dorsal horn in the rat: The forebrain. *J. Comp. Neurol.* *468*, 24–56.

- 651 Gross, C.T., and Canteras, N.S. (2012). The many paths to fear. *Nat. Rev. Neurosci.* *13*, 651–658.
- 652 Han, S., Soleiman, M.T., Soden, M.E., Zweifel, L.S., and Palmiter, R.D. (2015). Elucidating an Affective
653 Pain Circuit that Creates a Threat Memory. *Cell* *162*, 363–374.
- 654 Harriott, A.M., and Schwedt, T.J. (2014). Migraine is Associated With Altered Processing of Sensory
655 Stimuli. *Curr. Pain Headache Rep.* *18*, 458.
- 656 Harte, S.E., Ichesco, E., Hampson, J.P., Peltier, S.J., Schmidt-Wilcke, T., Clauw, D.J., and Harris, R.E.
657 (2016). Pharmacologic attenuation of cross-modal sensory augmentation within the chronic pain insula:
658 PAIN *157*, 1933–1945.
- 659 Helmstetter, F.J. (1992). The Amygdala Is Essential for the Expression of Conditional Hypoalgesia. *Behav.*
660 *Neurosci.* *106*, 518–528.
- 661 Huang, D., Grady, F.S., Peltekian, L., and Geerling, J.C. (2020). Efferent projections of VGLUT2 , FOXP2 , and
662 PDYN parabrachial neurons in mice. *J. Comp. Neurol.* *cne.24975*.
- 663 Hunt, S.P., and Mantyh, P.W. (2001). The molecular dynamics of pain control. *Nat. Rev. Neurosci.* *2*, 83–
664 91.
- 665 Hylden, J.L.K., Anton, F., and Nahin, R.L. (1989). Spinal lamina I projection neurons in the rat: Collateral
666 innervation of parabrachial area and thalamus. *Neuroscience* *28*, 27–37.
- 667 Janak, P.H., and Tye, K.M. (2015). From circuits to behaviour in the amygdala. *Nature* *517*, 284–292.
- 668 Julius, D., and Basbaum, A.I. (2001). Molecular mechanisms of nociception. *Nature* *413*, 203–210.
- 669 Kaur, S., Wang, J.L., Ferrari, L., Thankachan, S., Kroeger, D., Venner, A., Lazarus, M., Wellman, A.,
670 Arrigoni, E., Fuller, P.M., et al. (2017). A Genetically Defined Circuit for Arousal from Sleep during
671 Hypercapnia. *Neuron* *96*, 1153-1167.e5.
- 672 Kim, E.J., Jacobs, M.W., Ito-Cole, T., and Callaway, E.M. (2016). Improved Monosynaptic Neural Circuit
673 Tracing Using Engineered Rabies Virus Glycoproteins. *Cell Rep.* *15*, 692–699.
- 674 Kim, H., Mittal, D.P., Iadarola, M.J., and Dionne, R.A. (2006). Genetic predictors for acute experimental
675 cold and heat pain sensitivity in humans. *J. Med. Genet.* *43*, e40–e40.
- 676 Kim, J., Zhang, X., Muralidhar, S., LeBlanc, S.A., and Tonegawa, S. (2017). Basolateral to Central
677 Amygdala Neural Circuits for Appetitive Behaviors. *Neuron* *93*, 1464-1479.e5.
- 678 Klein, C. (2015). What Pain Asymbolia Really Shows. *Mind* *124*, 493–516.
- 679 Kunwar, P.S., Zelikowsky, M., Remedios, R., Cai, H., Yilmaz, M., Meister, M., and Anderson, D.J. (2015).
680 Ventromedial hypothalamic neurons control a defensive emotion state. *ELife* *4*, e06633.
- 681 Lampert, A., O'Reilly, A.O., Reeh, P., and Leffler, A. (2010). Sodium channelopathies and pain. *Pflüg.*
682 *Arch. - Eur. J. Physiol.* *460*, 249–263.
- 683 LeDoux, J. (2007). The amygdala. *Curr. Biol.* *17*, R868–R874.

- 684 LeDoux, J. (2012). Rethinking the Emotional Brain. *Neuron* 73, 653–676.
- 685 LeDoux, J.E. (2000). Emotion Circuits in the Brain. *Annu. Rev. Neurosci.* 23, 155–184.
- 686 LeDoux, J.E., Ruggiero, D.A., and Reis, D.J. (1985). Projections to the subcortical forebrain from
687 anatomically defined regions of the medial geniculate body in the rat. *J. Comp. Neurol.* 242, 182–213.
- 688 López-Solà, M., Woo, C.-W., Pujol, J., Deus, J., Harrison, B.J., Monfort, J., and Wager, T.D. (2017).
689 Towards a neurophysiological signature for fibromyalgia. *PAIN* 158, 34–47.
- 690 Manning, B.H., and Mayer, D.J. (1995). The central nucleus of the amygdala contributes to the
691 production of morphine antinociception in the formalin test. *PAIN*® 63, 141–152.
- 692 Maren, S. (2001). Neurobiology of Pavlovian Fear Conditioning. *Annu. Rev. Neurosci.* 24, 897–931.
- 693 McMurray, G.A. (1955). Congenital insensitivity to pain and its implications for motivational theory. *Can.*
694 *J. Psychol. Can. Psychol.* 9, 121–131.
- 695 Melzack, R., and Casey, K. (1968). Sensory, Motivational, and Central Control Determinants of Pain. In
696 *Skin Senses*, pp. 423–439.
- 697 Motta, S.C., Goto, M., Gouveia, F.V., Baldo, M.V.C., Canteras, N.S., and Swanson, L.W. (2009). Dissecting
698 the brain’s fear system reveals the hypothalamus is critical for responding in subordinate conspecific
699 intruders. *Proc. Natl. Acad. Sci.* 106, 4870–4875.
- 700 Nagasako, E.M., Oaklander, A.L., and Dworkin, R.H. (2003). Congenital insensitivity to pain: an update.
701 *PAIN* 101, 213–219.
- 702 Nantermet, P.G., and Henze, D.A. (2011). Recent Advances Toward Pain Therapeutics. In *Annual Reports*
703 *in Medicinal Chemistry*, (Elsevier), pp. 19–32.
- 704 Nassar, M.A., Stirling, L.C., Forlani, G., Baker, M.D., Matthews, E.A., Dickenson, A.H., and Wood, J.N.
705 (2004). Nociceptor-specific gene deletion reveals a major role for Nav1.7 (PN1) in acute and
706 inflammatory pain. *Proc. Natl. Acad. Sci.* 101, 12706–12711.
- 707 Neugebauer, V. (2015). Amygdala Pain Mechanisms. In *Pain Control*, (Springer, Berlin, Heidelberg), pp.
708 261–284.
- 709 Palmiter, R.D. (2018). The Parabrachial Nucleus: CGRP Neurons Function as a General Alarm. *Trends*
710 *Neurosci.* 41, 280–293.
- 711 Paues, J., Engblom, D., Mackerlova, L., Ericsson-Dahlstrand, A., and Blomqvist, A. (2001). Feeding-related
712 immune responsive brain stem neurons: association with CGRP. *NeuroReport* 12, 2399–2403.
- 713 Perl, E.R. (2007). Ideas about pain, a historical view. *Nat. Rev. Neurosci.* 8, 71–80.
- 714 Peschanski, M., Guilbaud, G., and Gautron, M. (1981). Posterior intralaminar region in rat: Neuronal
715 responses to noxious and nonnoxious cutaneous stimuli. *Exp. Neurol.* 72, 226–238.
- 716 Price, D.D. (1999). Multisensory integration in pain and consciousness. *Pain Forum* 8, 130–132.

- 717 Price, D.D. (2000). Psychological and Neural Mechanisms of the Affective Dimension of Pain. *Science*
718 *288*, 1769–1772.
- 719 Price, D.D. (2002). Central Neural Mechanisms that Interrelate Sensory and Affective Dimensions of
720 Pain. *Mol. Interv.* *2*, 392.
- 721 Ren, W., and Neugebauer, V. (2010). Pain-related increase of excitatory transmission and decrease of
722 inhibitory transmission in the central nucleus of the amygdala are mediated by mGluR1. *Mol. Pain* *6*, 93.
- 723 Ressler, R.L., and Maren, S. (2019). Synaptic encoding of fear memories in the amygdala. *Curr. Opin.*
724 *Neurobiol.* *54*, 54–59.
- 725 Rosen, J.B., Asok, A., and Chakraborty, T. (2015). The smell of fear: innate threat of 2,5-dihydro-2,4,5-
726 trimethylthiazoline, a single molecule component of a predator odor. *Front. Neurosci.* *9*.
- 727 Russell, F.A., King, R., Smillie, S.-J., Kodji, X., and Brain, S.D. (2014). Calcitonin Gene-Related Peptide:
728 Physiology and Pathophysiology. *Physiol. Rev.* *94*, 1099–1142.
- 729 Russo, A.F. (2015). Calcitonin Gene-Related Peptide (CGRP): A New Target for Migraine. *Annu. Rev.*
730 *Pharmacol. Toxicol.* *55*, 533–552.
- 731 Salay, L.D., Ishiko, N., and Huberman, A.D. (2018). A midline thalamic circuit determines reactions to
732 visual threat. *Nature* *557*, 183.
- 733 Sanz, E., Yang, L., Su, T., Morris, D.R., McKnight, G.S., and Amieux, P.S. (2009). Cell-type-specific isolation
734 of ribosome-associated mRNA from complex tissues. *Proc. Natl. Acad. Sci.* *106*, 13939–13944.
- 735 Sato, M., Ito, M., Nagase, M., Sugimura, Y.K., Takahashi, Y., Watabe, A.M., and Kato, F. (2015). The
736 lateral parabrachial nucleus is actively involved in the acquisition of fear memory in mice. *Mol. Brain* *8*,
737 *22*.
- 738 Shang, C., Chen, Z., Liu, A., Li, Y., Zhang, J., Qu, B., Yan, F., Zhang, Y., Liu, W., Liu, Z., et al. (2018).
739 Divergent midbrain circuits orchestrate escape and freezing responses to looming stimuli in mice. *Nat.*
740 *Commun.* *9*, 1232.
- 741 Shinohara, K., Watabe, A.M., Nagase, M., Okutsu, Y., Takahashi, Y., Kurihara, H., and Kato, F. (2017).
742 Essential role of endogenous calcitonin gene-related peptide in pain-associated plasticity in the central
743 amygdala. *Eur. J. Neurosci.* *46*, 2149–2160.
- 744 Silva, B.A., Mattucci, C., Krzywkowski, P., Murana, E., Illarionova, A., Grinevich, V., Canteras, N.S.,
745 Ragozzino, D., and Gross, C.T. (2013). Independent hypothalamic circuits for social and predator fear.
746 *Nat. Neurosci.* *16*, 1731–1733.
- 747 Silva, B.A., Gross, C.T., and Gräff, J. (2016). The neural circuits of innate fear: detection, integration,
748 action, and memorization. *Learn. Mem.* *23*, 544–555.
- 749 Simons, L.E., Moulton, E.A., Linnman, C., Carpino, E., Becerra, L., and Borsook, D. (2014). The human
750 amygdala and pain: Evidence from neuroimaging. *Hum. Brain Mapp.* *35*, 527–538.

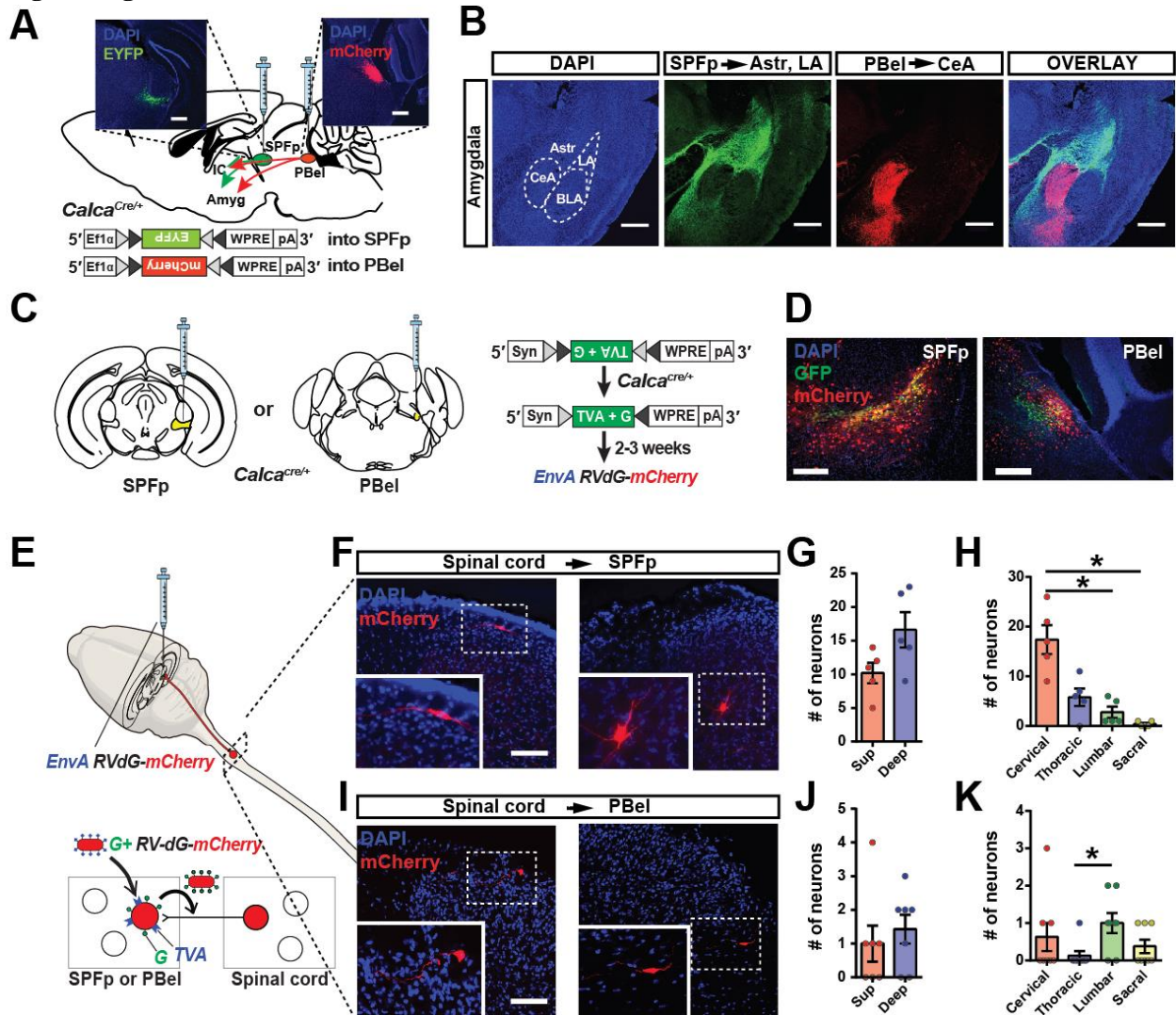
- 751 Stamatakis, A.M., and Stuber, G.D. (2012). Activation of lateral habenula inputs to the ventral midbrain
752 promotes behavioral avoidance. *Nat. Neurosci.* *15*, 1105–1107.
- 753 Tanimoto, S., Nakagawa, T., Yamauchi, Y., Minami, M., and Satoh, M. (2003). Differential contributions
754 of the basolateral and central nuclei of the amygdala in the negative affective component of chemical
755 somatic and visceral pains in rats. *Eur. J. Neurosci.* *18*, 2343–2350.
- 756 Thompson, J.M., and Neugebauer, V. (2017). Amygdala Plasticity and Pain. *Pain Res. Manag.* *2017*.
- 757 Todd, A.J. (2010). Neuronal circuitry for pain processing in the dorsal horn. *Nat. Rev. Neurosci.* *11*, 823–
758 836.
- 759 Tong, W.H., Abdulai-Saiku, S., and Vyas, A. (2020). Medial Amygdala Arginine Vasopressin Neurons
760 Regulate Innate Aversion to Cat Odors in Male Mice. *Neuroendocrinology*.
- 761 Veinante, P., Yalcin, I., and Barrot, M. (2013). The amygdala between sensation and affect: a role in pain.
762 *J. Mol. Psychiatry* *1*.
- 763 Wang, L., Gillis-Smith, S., Peng, Y., Zhang, J., Chen, X., Salzman, C.D., Ryba, N.J.P., and Zuker, C.S. (2018).
764 The coding of valence and identity in the mammalian taste system. *Nature* *558*, 127–131.
- 765 Wei, P., Liu, N., Zhang, Z., Liu, X., Tang, Y., He, X., Wu, B., Zhou, Z., Liu, Y., Li, J., et al. (2015). Processing
766 of visually evoked innate fear by a non-canonical thalamic pathway. *Nat. Commun.* *6*, 6756.
- 767 Willis, W.D., Zhang, X., Honda, C.N., and Giesler, G.J. (2002). A critical review of the role of the proposed
768 VMpo nucleus in pain. *J. Pain* *3*, 79–94.
- 769 Xiong, X.R., Liang, F., Zingg, B., Ji, X., Ibrahim, L.A., Tao, H.W., and Zhang, L.I. (2015). Auditory cortex
770 controls sound-driven innate defense behaviour through corticofugal projections to inferior colliculus.
771 *Nat. Commun.* *6*, 7224.
- 772 Xiu, J., Zhang, Q., Zhou, T., Zhou, T., Chen, Y., and Hu, H. (2014). Visualizing an emotional valence map in
773 the limbic forebrain by TAI-FISH. *Nat. Neurosci.* *17*, 1552–1559.
- 774 Yasui, Y., Saper, C.B., and Ceppetto, D.F. (1991). Calcitonin gene-related peptide (CGRP) immunoreactive
775 projections from the thalamus to the striatum and amygdala in the rat. *J. Comp. Neurol.* *308*, 293–310.
- 776 Yeh, L.-F., Watanabe, M., Sulkes-Cuevas, J., and Johansen, J.P. (2018). Dysregulation of aversive signaling
777 pathways: a novel circuit endophenotype for pain and anxiety disorders. *Curr. Opin. Neurobiol.* *48*, 37–
778 44.
- 779 Yokota, S., Kaur, S., VanderHorst, V.G., Saper, C.B., and Chamberlin, N.L. (2015). Respiratory-related
780 outputs of glutamatergic, hypercapnia-responsive parabrachial neurons in mice. *J. Comp. Neurol.* *523*,
781 907–920.
- 782 Yu, L.-C., Hou, J.-F., Fu, F.-H., and Zhang, Y.-X. (2009). Roles of calcitonin gene-related peptide and its
783 receptors in pain-related behavioral responses in the central nervous system. *Neurosci. Biobehav. Rev.*
784 *33*, 1185–1191.

785 Zhang, X., and Giesler, G.J. (2005). Response Characteristics of Spinothalamic Tract Neurons That Project
786 to the Posterior Thalamus in Rats. *J. Neurophysiol.* *93*, 2552–2564.

787 Zhou, Z., Liu, X., Chen, S., Zhang, Z., Liu, Y., Montardy, Q., Tang, Y., Wei, P., Liu, N., Li, L., et al. (2019). A
788 VTA GABAergic Neural Circuit Mediates Visually Evoked Innate Defensive Responses. *Neuron* *103*, 473-
789 488.e6.

790

791 **Figure Legends**



792 **Figure 1. CGRP^{SPFp} and CGRP^{PBel} neurons form spino-thalamo-amygdaloid and spino-parabrachio-**
 793 **amygdaloid pathways.**
 794

795 (A) Schematic and representative images of Cre-dependent expression of EYFP in the SPFp and mCherry
 796 in the PBel of a *Calca*^{Cre} mouse. Scale bars, 200 μ m.

797 (B) The axonal projections from the CGRP^{SPFp} and CGRP^{PBel} neurons are mutually exclusive in the
 798 amygdala sub-regions. Scale bars, 500 μ m.

799 (C) Schematic diagrams and images of Cre-dependent expression of TVA and G in SPFp or PBel neurons
 800 of *Calca*^{Cre} mice for the rabies tracing.

801 (D) Representative images of the SPFp and PBel five days after EnvA-RVdG-mCherry injection. Yellow
 802 indicates the starter cells. Scale bars, 200 μ m.

803 (E) A schematic diagram of identifying presynaptic neurons by monosynaptic rabies tracing.

804 (F) Representative images of superficial and deep layer dorsal horn neurons that project to CGRP^{SPFp}
 805 neurons.

806 (G) The number of spinal dorsal horn neurons in the superficial (Sup) and deep (deep) layers project to the
 807 CGRP^{SPFp} neurons.

808 (H) The number of spinal cord neurons in different spinal segments that project to the CGRP^{SPFP} neurons.

809 (I) Representative images of the superficial dorsal horn and lateral spinal nucleus neurons project to
810 CGRP^{PBel} neurons.

811 (J) The number of spinal dorsal horn neurons in the superficial (Sup) and deep (deep) layers project to the
812 CGRP^{PBel} neurons.

813 (K) The number of spinal cord neurons in different spinal segments that project to the CGRP^{PBel} neurons.

814

815

816 **Statistics**

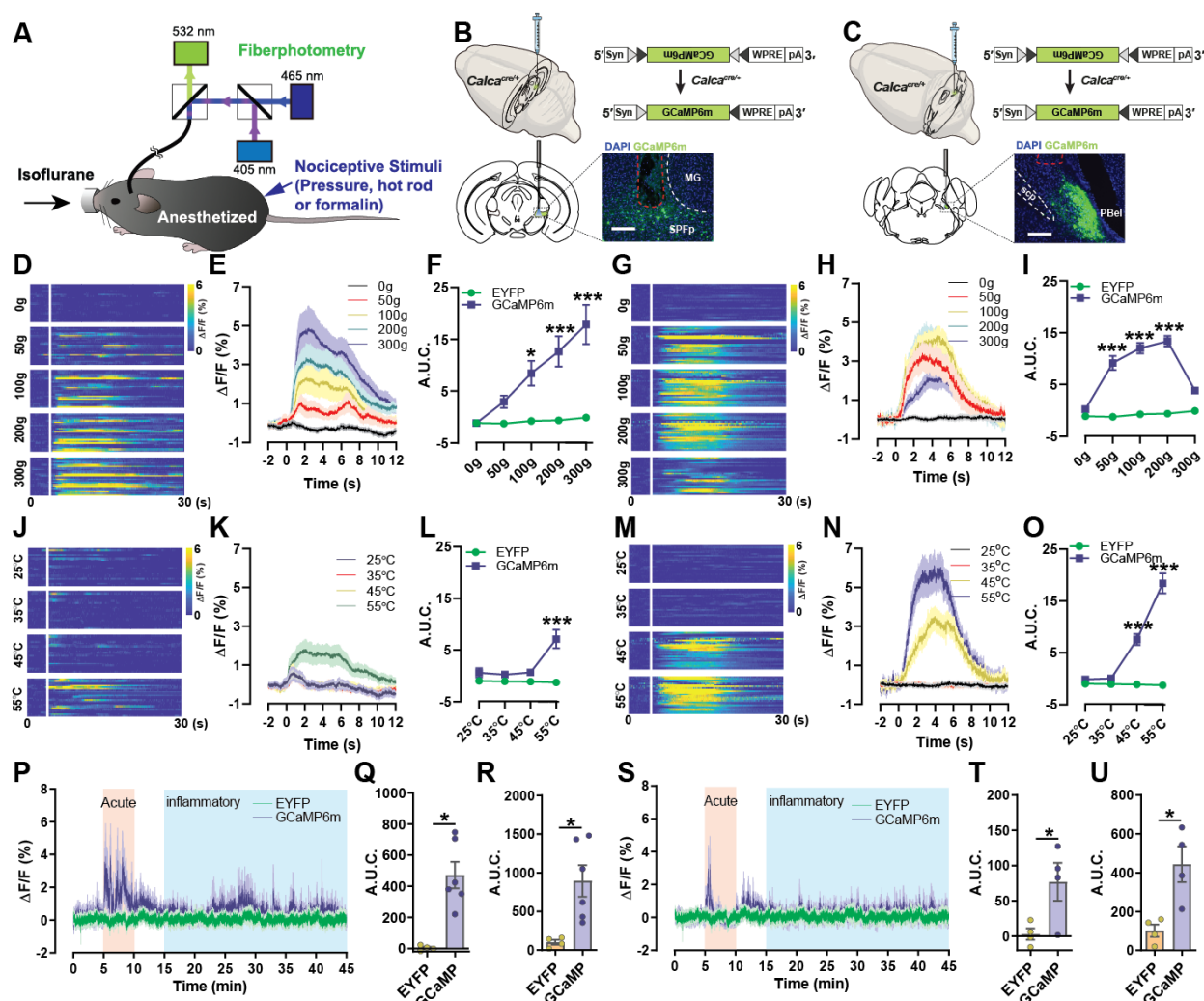
817 (G) Superficial: 10.20 ± 1.53 , Deep: 16.60 ± 2.62 (n = 5). Paired t-test (two-tailed), p = 0.0723.

818 (H) Cervical: 17.40 ± 2.91 , Thoracic: 5.80 ± 2.91 , Lumbar: 2.80 ± 1.11 , Sacral: 0.40 ± 0.24 (n = 5). Repeated
819 measure one-way ANOVA, p = 0.0017. Cervical group was significantly different with lumbar (p < 0.05)
820 and sacral (p < 0.05, Tukey's multiple comparisons).

821 (J) Superficial: 1.00 ± 0.53 , Deep: 1.43 ± 0.43 (n = 8). Paired t-test (two-tailed), p = 0.6286.

822 (K) Cervical: 0.63 ± 0.38 , Thoracic: 0.13 ± 0.13 , Lumbar: 1.00 ± 0.27 , Sacral: 0.38 ± 0.18 (n = 8). Repeated
823 measure one-way ANOVA, p = 0.1615. Thoracic group was significantly different with lumbar (p < 0.05,
824 Tukey's multiple comparisons).

825



826
 827 **Figure 2. CGRP^{SPFp} and CGRP^{PBel} neurons are activated by multimodal nociceptive stimuli.**
 828 (A) A diagram of the fiber photometry calcium imaging experiment in an anesthetized mouse.
 829 (B, and C) A schematic and representative image of the Cre-dependent expression of GCaMP6m in the
 830 *Calca^{Cre}* mice with an optical fiber implanted (red dashed line in the overlay image indicates fiber track)
 831 above the SPFp and PBel. Scale bars, 200 μ m.
 832 (D-F) Intensity-dependent calcium activity increase in CGRP^{SPFp} neurons in response to a pressure meter
 833 (0, 50, 100, 200, and 300 g).
 834 (G-I) Intensity-dependent calcium activity increase in CGRP^{PBel} neurons to a pressure meter.
 835 (J-L) Intensity-dependent calcium activity increase in CGRP^{SPFp} neurons in response to a temperature-controlled
 836 rod (25, 35, 45, or 55 °C).
 837 (M-O) Intensity-dependent calcium activity increase in CGRP^{PBel} neurons in response to a temperature-
 838 controlled rod.
 839 (P) Calcium signal increases in CGRP^{SPFp} neurons following subcutaneous injection of formalin (4%) into
 840 the paw.
 841 (Q) Area under curve (A.U.C.) quantification of the CGRP^{SPFp} neuronal activity during the acute phase (5–
 842 10 min) of formalin response.

843 (R) A.U.C. quantification of the CGRP^{SPFP} neuronal activity during the inflammatory phase (15–45 min)
844 of formalin injection.

845 (S) Calcium signal increases in CGRP^{PBel} neurons in response to subcutaneous injection of formalin (4%)
846 into the paw.

847 (T) A.U.C. quantification of the CGRP^{PBel} neuronal activity during the acute phase (5–10 min) of formalin
848 response.

849 (U) A.U.C. quantification of the CGRP^{PBel} neuronal activity during the inflammatory phase (15–45 min) of
850 formalin response.

851

852

853 **Statistics**

854 (F) Repeated measure two-way ANOVA showed significance in interaction ($F(4, 152) = 9.838, p < 0.0001$),
855 intensity ($F(4, 152) = 12.28, p < 0.0001$) and group ($F(1, 38) = 16.01, p = 0.0003$). 100 ($p < 0.05$), 200 (p
856 < 0.0001) and 300 g ($p < 0.0001$) points were significantly different between EYFP and GCaMP6m with
857 Sidak's multiple comparisons test.

858 (I) Repeated measure two-way ANOVA showed significance in interaction ($F(4, 248) = 15.08, p < 0.0001$),
859 intensity ($F(4, 248) = 15.17, p < 0.0001$) and group ($F(1, 62) = 64.40, p < 0.0001$). 50 ($p < 0.0001$), 100
860 ($p < 0.0001$) and 200 g ($p < 0.0001$) points were significantly different between EYFP and GCaMP6m with
861 Sidak's multiple comparisons test.

862 (L) Repeated measure two-way ANOVA showed significance in interaction ($F(3, 114) = 10.97, p < 0.0001$),
863 intensity ($F(3, 114) = 9.61, p < 0.0001$) and group ($F(1, 38) = 11.12, p = 0.0019$). 55°C ($p < 0.0001$) was
864 significantly different between EYFP and GCaMP6m with Sidak's multiple comparisons test.

865 (M) Repeated measure two-way ANOVA showed significance in interaction ($F(3, 186) = 23.96, p <$
866 0.0001), intensity ($F(3, 186) = 22.67, p < 0.0001$) and group ($F(1, 62) = 46.05, p < 0.0001$). 45 and 55°C
867 (both $p < 0.0001$) points were significantly different between EYFP and GCaMP6m with Sidak's multiple
868 comparisons test.

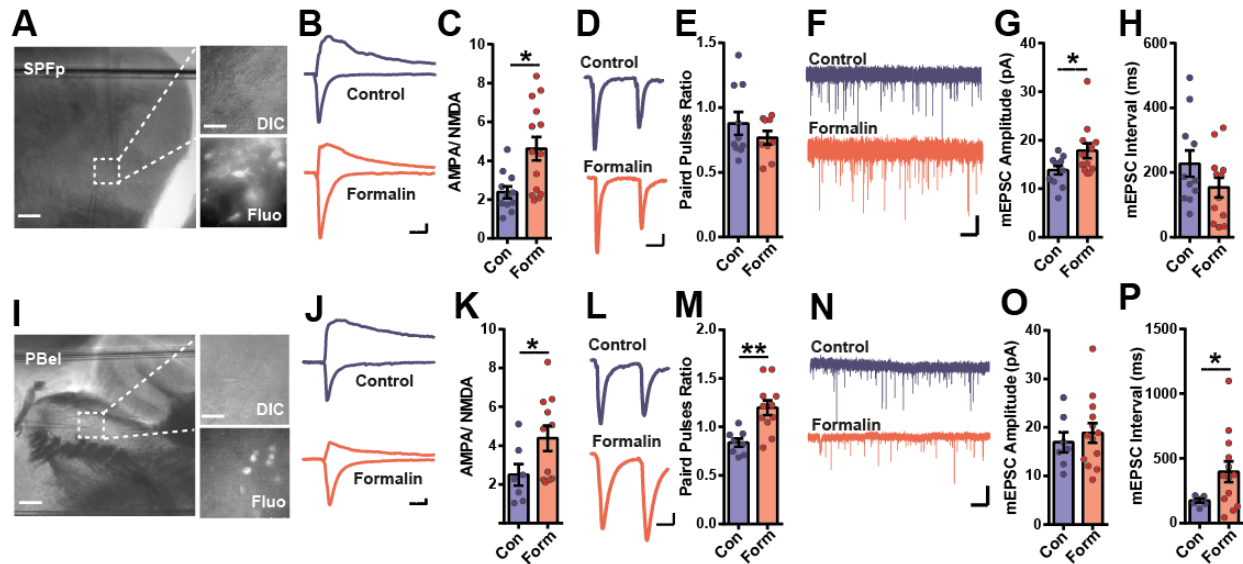
869 (Q) EYFP: 2.86 ± 8.00 ($n = 4$ mice), GCaMP6m: 471.9 ± 85.53 ($n = 6$ mice). Unpaired t-test (two-tailed),
870 $p = 0.0024$.

871 (R) EYFP: 100.60 ± 31.89 ($n = 4$), GCaMP6m: 894.80 ± 203.40 ($n = 6$). Unpaired t-test (two-tailed), $p =$
872 0.0145 .

873 (K) EYFP: 6.18 ± 4.05 ($n = 4$), GCaMP6m: 77.00 ± 26.83 ($n = 4$). Unpaired t-test (two-tailed), $p = 0.0381$.

874 (L) EYFP: 100.60 ± 31.89 ($n = 4$), GCaMP6m: 443.50 ± 92.46 ($n = 4$). Unpaired t-test (two-tailed), $p =$
875 0.0127 .

876



877
 878 **Figure 3. Pain-induced synaptic plasticity changes in CGRP^{SPFp} and CGRP^{PBel} neurons.**
 879 (A) A representative image of a brain slice including SPFp used for the whole-cell patch clamp experiment.
 880 Enlarged images show the fluorescence from Cre:GFP-expressing CGRP neurons. Scale bars, 100 μ m in
 881 left images, and 10 μ m in enlarged images.
 882 (B) Example traces of AMPA and NMDA EPSCs in control (blue) and formalin (red) injected groups. Scale
 883 bars, 20 ms, and 50 pA.
 884 (C) The AMPA/NMDA ratio was increased in the formalin injected group compared with the control group.
 885 (D, and E) No significant differences in paired pulse ratio were observed between the formalin-injected
 886 group and the control group. Scale bars, 20 ms, and 50 pA.
 887 (F) Example traces of mEPSCs in control (blue) and formalin (red) injected group. Scale bars, 1 s, and 20
 888 pA.
 889 (G) mEPSC amplitude was increased in the formalin injected group compared with the control group.
 890 (H) mEPSC interval was not changed in the formalin injected group compared with the control group.
 891 (I) A representative image of a brain slice including PBel for the whole-cell patch clamp experiment.
 892 Enlarged images are the PBel cells with and without fluorescence. Cells with fluorescence are CGRP
 893 neurons. Scale bars, 100 μ m in left images, and 10 μ m in enlarged images.
 894 (J) Example traces of AMPA and NMDA EPSCs in control (blue) and formalin (red) injected groups. Scale
 895 bars, 20 ms, and 20 pA.
 896 (K) The AMPA/NMDA ratio was increased in the formalin injected group compared with the control group.
 897 (L, and M) The formalin injected group display an increased paired pulse ratio compared to the control
 898 group. Scale bars, 20 ms, and 50 pA.
 899 (N) Example traces of mEPSCs in the control (blue) and formalin (red) injected group. Scale bars. 1 s and
 900 50 pA.
 901 (O) mEPSC amplitude was not changed in the formalin injected group compared with the control group.
 902 (P) mEPSC interval increased in the formalin injected group compared with the control group.

903
 904
 905
 906

907 **Statistics**

908 (C) SPFP; Control: 2.38 ± 0.31 (n = 11 cells), formalin: 4.62 ± 0.61 (n = 14 cells). Unpaired t test (two-
909 tailed), p = 0.0063.

910 (E) SPFP; Control: 0.88 ± 0.09 (n = 10 cells), formalin: 0.77 ± 0.05 (n = 9 cells). Unpaired t test (two-
911 tailed), p = 0.2957.

912 (G) SPFP; Control: 13.81 ± 0.90 (n = 11 cells), formalin: 17.83 ± 1.56 (n = 12 cells). Unpaired t test (two-
913 tailed), p = 0.0390.

914 (H) SPFP; Control: 227.4 ± 40.90 (n = 11 cells), formalin: 154.2 ± 30.80 (n = 12 cells). Unpaired t test
915 (two-tailed), p = 0.1687.

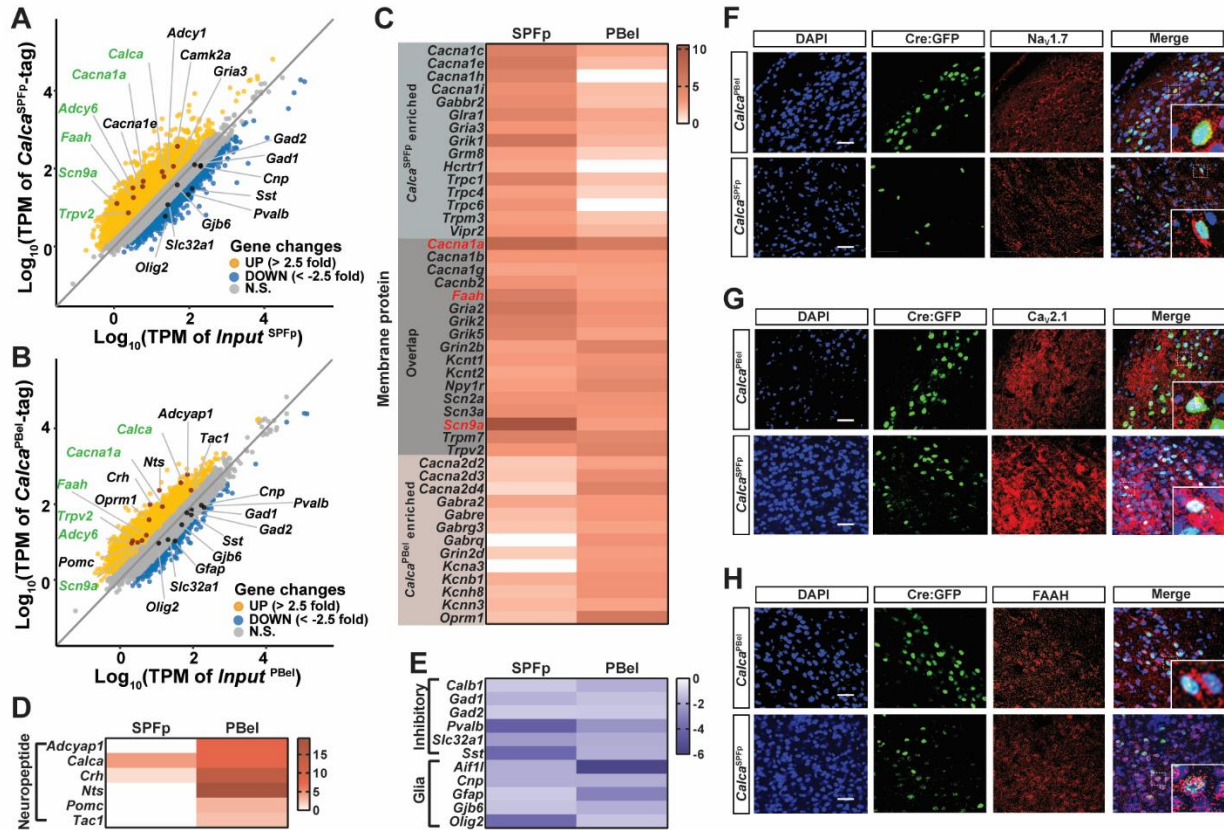
916 (K) PBel; Control: 2.49 ± 0.56 (n = 7 cells), formalin: 4.38 ± 0.65 (n = 11 cells). Unpaired t test (two-tailed),
917 p = 0.0437.

918 (M) PBel; Control: 0.84 ± 0.04 (n = 8 cells), formalin: 1.20 ± 0.77 (n = 11 cells). Unpaired t test (two-
919 tailed), p = 0.001.

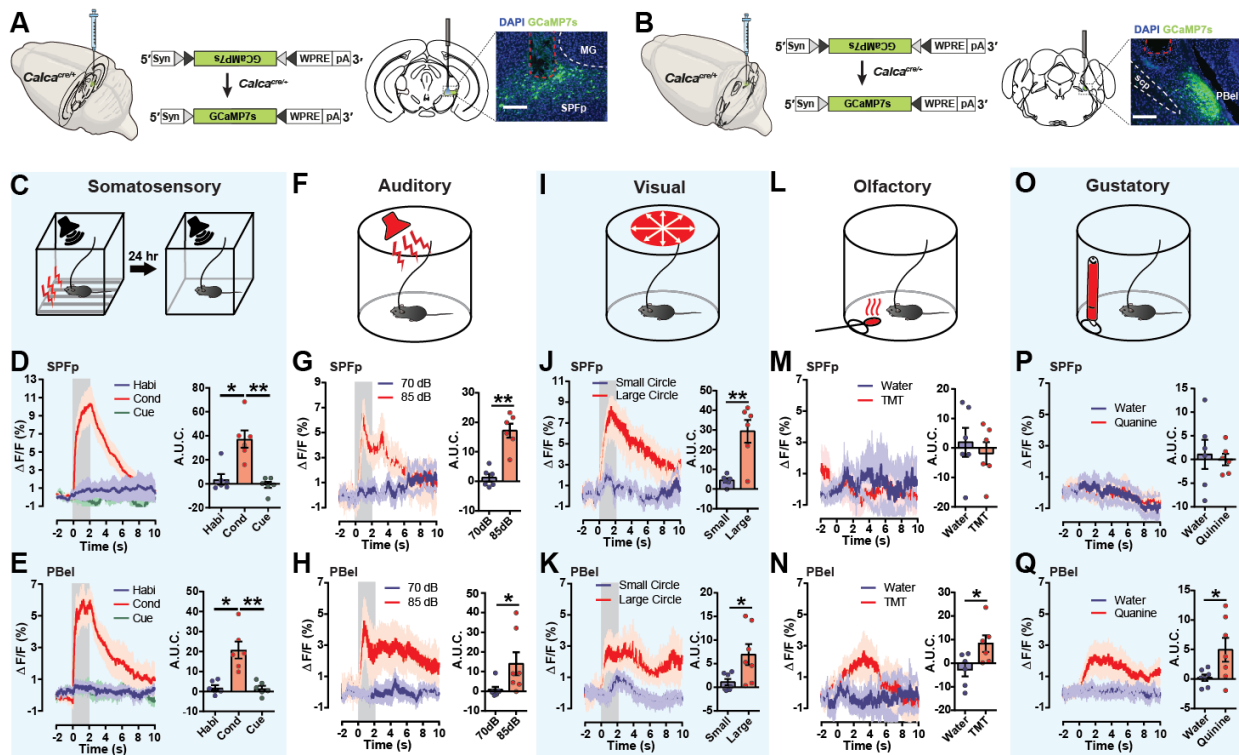
920 (O) PBel; Control: 16.93 ± 2.08 (n = 7 cells), formalin: 18.85 ± 2.04 (n = 13 cells). Unpaired t test (two-
921 tailed), p = 0.5196.

922 (P) PBel; Control: 173.2 ± 13.89 (n = 7 cells), formalin: 396.5 ± 80.66 (n = 13 cells). Unpaired t test (two-
923 tailed), p = 0.0175.

924



925
 926 **Figure 4. Active transcriptome profiling of CGRP^{SPFp} and CGRP^{PBel} neurons.**
 927 (A) Correlation plot showing expression (transcript per million, TPM in log 10 scale) of genes enriched in
 928 CGRP^{SPFp} neurons compared with the total SPFp inputs using RiboTag transcriptome profiling. Up and
 929 down-regulated genes were separated based on 2.5 or -2.5-fold enrichment.
 930 (B) Correlation plot of the transcriptome profiles of CGRP^{PBel} neurons versus total PBel inputs.
 931 (C) Heatmaps showing fold changes of genes in the SPFp and PBel that encode membrane proteins.
 932 (D) Heatmaps showing fold changes of genes in the SPFp and PBel that encode neuropeptides,
 933 (E) Heatmaps showing fold changes of genes in the SPFp and PBel that encode markers of inhibitory neuron
 934 or glia.
 935 (F-H) Co-expression of Nav1.7 (F), Cav2.1 (G), or FAAH (H) with CGRP by double IHC. Scale bars, 50
 936 μm .



937

938 **Figure 5. CGRP^{SPFP} and CGRP^{PBel} neurons are activated by multimodal sensory threat stimuli.**

939 (A, and B) A schematic and representative images of Cre-dependent expression of GCaMP7s in the
 940 CGRP^{SPFP} (A) and CGRP^{PBel} (B) neurons for fiber photometry. Scale bars, 200 μ m.

941 (C) Cued fear conditioning test with low volume tone (72 dB) was performed to examine the responses of
 942 CGPR neurons to the somatosensory aversive stimulus (2-s, 0.6 mA electric foot shock).

943 (D, and E) CGRP^{SPFP} (D) and CGRP^{PBel} (E) neurons were activated by the electric foot shock during the
 944 conditioning period, but not habituation, nor the cued retrieval period. Left, averaged calcium traces. Right,
 945 A.U.C. quantification.

946 (F) Intense sound (85 dB) was used as an aversive auditory stimulus, with a 70-dB low-intensity sound as a
 947 control.

948 (G, and H) CGRP^{SPFP} (G) and CGRP^{PBel} (H) neurons were activated by the intense sound. Left, averaged
 949 calcium traces. Right, A.U.C. quantification.

950 (I) A large looming disk was used as an aversive visual stimulus, with a small disk as a control.

951 (J, and K) CGRP^{SPFP} (J) and CGRP^{PBel} (K) neurons were activated by the large looming disk. Left,
 952 averaged calcium traces. Right, A.U.C. quantification.

953 (L) TMT-soaked cotton was used as an aversive olfactory stimulus, with water as a control.

954 (M) There was no activity change in CGRP^{SPFP} neurons when the animal approached the TMT-soaked
 955 cotton. Left, averaged calcium traces. Right, A.U.C. quantification.

956 (N) CGRP^{PBel} neurons were activated when the animal approached the TMT-soaked cotton.. Left, averaged
 957 calcium traces. Right, A.U.C. quantification.

958 (O) Quinine solution (0.5 mM) was introduced as an aversive gustatory stimulus (water was the control).

959 (P) Quinine did not affect CGRP^{SPFP} neurons. Left, averaged calcium traces. Right, A.U.C. quantification.

960 (Q) CGRP^{PBel} neurons were activated by quinine solution (0.5 mM). Left, averaged calcium traces. Right,
 961 A.U.C. quantification.

962

963 **Statistics**

964 (D) SPFP; Habituation: 3.63 ± 4.45 , conditioning: 37.31 ± 7.18 , cue test: -0.92 ± 2.57 ($n = 6$). Repeated
965 measure one-way ANOVA, $p = 0.0029$. Conditioning was significantly different with habituation ($p < 0.05$)
966 and cue test ($p < 0.01$, Tukey's multiple comparisons).

967 (E) PBel; SPFP; Habituation: 1.85 ± 1.33 , conditioning: 20.73 ± 4.25 , cue test: 1.49 ± 1.35 ($n = 6$). Repeated
968 measure one-way ANOVA, $p = 0.0022$. Conditioning was significantly different with habituation ($p < 0.05$)
969 and cue test ($p < 0.01$, Tukey's multiple comparisons).

970 (G) SPFP; 70 dB: 1.226 ± 1.27 , 85 dB: 17.14 ± 2.38 ($n = 6$). Paired t test (two-tailed), $p = 0.0018$.

971 (H) PBel; 70 dB: 0.78 ± 1.46 , 85 dB: 14.06 ± 5.86 ($n = 7$). Paired t test (two-tailed), $p = 0.0437$.

972 (J) SPFP; Small disk: 4.41 ± 1.11 , large disk: 29.30 ± 5.81 ($n = 6$). Paired t test (two-tailed), $p = 0.0091$.

973 (K) PBel; Small disk: 1.08 ± 0.69 , large disk: 6.93 ± 2.23 ($n = 7$). Paired t test (two-tailed), $p = 0.0357$.

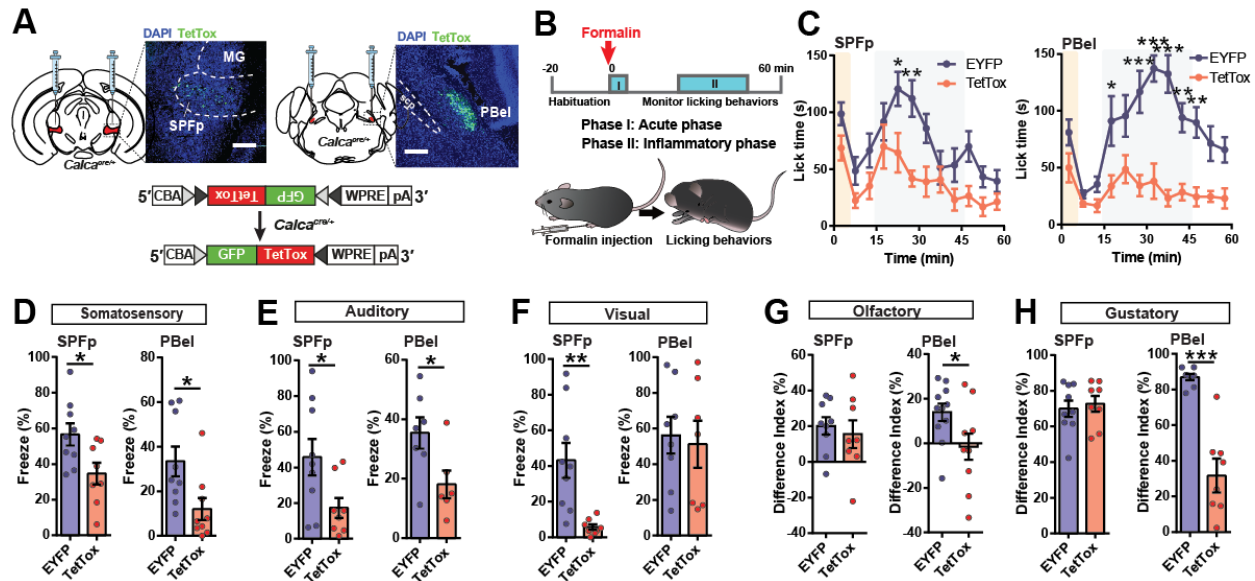
974 (M) SPFP; Water: 1.93 ± 4.88 , TMT: -1.82 ± 3.78 ($n = 6$). Paired t test (two-tailed), $p = 0.4411$.

975 (N) PBel; Water: -2.72 ± 2.84 , TMT: 8.28 ± 3.57 ($n = 6$). Paired t test (two-tailed), $p = 0.0145$.

976 (P) SPFP; Water: 1.10 ± 3.09 , quinine: -0.01 ± 1.22 ($n = 6$). Paired t test (two-tailed), $p = 0.7707$.

977 (Q) PBel; Water: 0.2209 ± 0.83 , quinine: 4.96 ± 2.01 ($n = 7$). Paired t test (two-tailed), $p = 0.0377$.

978



979
980 **Figure 6. Silencing CGRP^{SPFP} or CGRP^{PBel} neuronal activities attenuates perception of affective pain**
981 **and multisensory threat stimuli.**

982 (A) Schematics and representative images of Cre-dependent TetTox expression targeting CGRP^{SPFP} or
983 CGRP^{PBel} neurons. Scale bars, 200 μ m.

984 (B) A schematic diagram of the Formalin assay to test inflammatory pain responses.

985 (C) The CGRP^{SPFP} and CGRP^{PBel} silenced groups displayed significantly alleviated inflammatory pain
986 responses.

987 (D) Both the CGRP^{SPFP} and CGRP^{PBel} silenced groups froze less in response to electric foot shock (2-s, 0.6
988 mA) compared to controls.

989 (E) Both the CGRP^{SPFP} and CGRP^{PBel} silenced groups froze less in response to 85-dB intense sound
990 compared with controls.

991 (F) In response to a looming aversive visual stimulus, the CGRP^{SPFP} silenced group showed less freezing,
992 whereas there was no difference between EYFP and CGRP^{PBel} silenced groups.

993 (G) A two-chamber choice test with TMT- and water-soaked cotton placed at each corner of the chamber
994 was used to test animals' responses to aversive olfactory stimulus. The CGRP^{SPFP} silenced group, and EYFP
995 controls both avoided the TMT chamber, while the CGRP^{PBel} TetTox group exhibited less aversion to TMT,
996 spending equal amounts of time in the water and TMT chambers.

997 (H) Quinine solution (0.5 mM) and water choice test was performed to test the animals' responses to
998 aversive gustatory stimulus. There was no change in water preference in the CGRP^{SPFP} silenced group, but
999 the CGRP^{PBel} silenced group showed a lower difference index than the control group.

1000

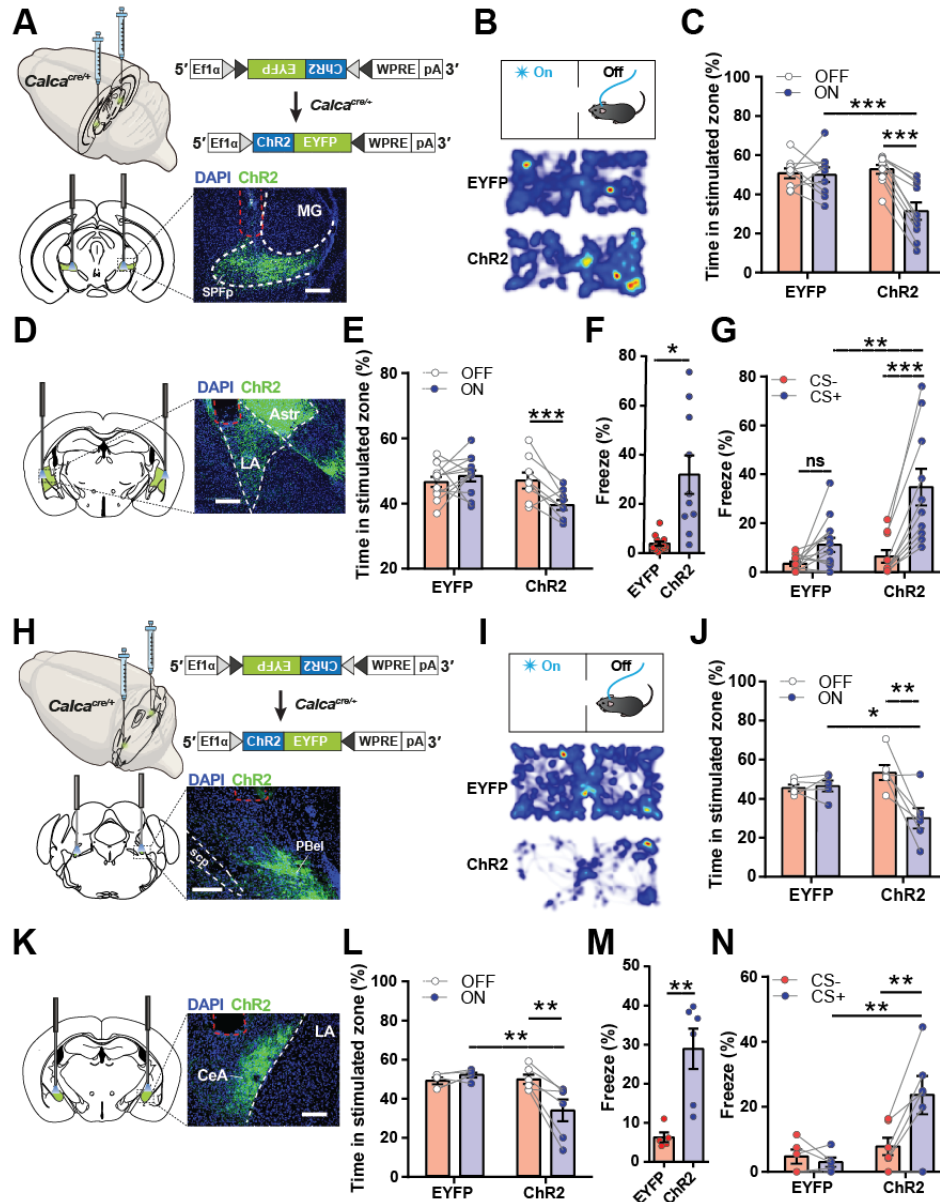
1001

1002 Statistics

1003 (C) SPFP: Repeated measure two-way ANOVA showed no significance in interaction ($F(11, 187) = 1.32$,
1004 $p = 0.2148$), but in time ($F(11, 187) = 9.05$, $p < 0.0001$) and group ($F(1, 17) = 9.57$, $p = 0.0066$). 20-25 (p
1005 < 0.05) and 25-30 ($p < 0.01$) min point were significantly different between EYFP and TetTox with Sidak's
1006 multiple comparisons test.

1007 PBel: Repeated measure two-way ANOVA showed significance in interaction ($F(11, 187) = 3.45$, $p =$
1008 0.0002), time ($F(11, 187) = 5.97$, $p < 0.0001$) and group ($F(1, 17) = 53.24$, $p < 0.0001$). 15-20 ($p < 0.05$),

1009 25-30 ($p < 0.0001$), 30-35 ($p < 0.0001$), 35-40 ($p < 0.0001$), 40-45 ($p < 0.01$), 45-50 ($p < 0.01$) min point
1010 were significantly different between EYFP and TetTox with Sidak's multiple comparisons test.
1011 (D) SPFP; EYFP: 56.62 ± 6.21 % ($n = 9$), TetTox: 34.65 ± 6.11 % ($n = 8$). Unpaired t test (two-tailed), $p =$
1012 0.0240 .
1013 PBel; EYFP: 33.43 ± 6.66 % ($n = 9$), TetTox: 12.04 ± 4.88 % ($n = 9$). Unpaired t test (two-tailed), $p =$
1014 0.0197 .
1015 (E) SPFP; EYFP: 45.74 ± 10.26 % ($n = 9$), TetTox: 17.32 ± 5.58 % ($n = 8$). Unpaired t test (two-tailed), $p =$
1016 0.0332 .
1017 PBel; EYFP: 35.39 ± 5.29 % ($n = 7$), TetTox: 18.14 ± 4.66 % ($n = 6$). Unpaired t test (two-tailed), $p =$
1018 0.0350 .
1019 (F) SPFP; EYFP: 43.12 ± 9.82 % ($n = 9$), TetTox: 5.73 ± 1.57 % ($n = 8$). Unpaired t test (two-tailed), $p =$
1020 0.0029 .
1021 PBel; EYFP: 56.20 ± 10.33 % ($n = 8$), TetTox: 51.22 ± 13.21 % ($n = 7$). Unpaired t test (two-tailed), $p =$
1022 0.0029 .
1023 (G) SPFP; EYFP: 20.12 ± 4.91 % ($n = 9$), TetTox: 15.55 ± 7.75 % ($n = 8$). Unpaired t test (two-tailed), $p =$
1024 0.6175 .
1025 PBel; EYFP: 13.87 ± 3.94 % ($n = 11$), TetTox: -1.53 ± 5.89 % ($n = 10$). Unpaired t test (two-tailed), $p =$
1026 0.0396 .
1027 (H) SPFP; EYFP: 69.96 ± 4.64 % ($n = 9$), TetTox: 72.66 ± 4.48 % ($n = 8$). Unpaired t test (two-tailed), $p =$
1028 0.6823 .
1029 PBel; EYFP: 86.87 ± 1.77 % ($n = 8$), TetTox: 31.66 ± 9.45 % ($n = 7$). Unpaired t test (two-tailed), $p <$
1030 0.0001 .
1031



1032

1033

Figure 7. Activating the CGRP^{SPFp→LA} or CGRP^{PBel→CeA} pathways encodes negative valence.

1034 (A) Schematics and representative image of Cre-dependent expression of ChR2 in the SPFp of *Calca^{Cre}*
 1035 mice and optic fiber placement (red dotted line).

1036 (B) A schematic diagram and heatmap of the real-time place aversion (RTPA) test with CGRP^{SPFp} cell body
 1037 stimulation.

1038 (C) Time spent in the stimulated zone during the RTPA test.

1039 (D) Representative image of optic fiber placement in the LA for terminal stimulation (red dotted line).

1040 (E) Time spent in the stimulated zone during the RTPA test with CGRP^{SPFp→LA} terminal stimulation.

1041 (F) Time spent freezing during the context test.

1042 (G) Time spent freezing during cue test after pairing optical stimulation and tone for cued fear conditioning.

1043 (H) Schematic and representative image of Cre-dependent expression of ChR2 in the PBel of *Calca^{Cre}* mice
 1044 and optic fiber placement (red dotted line).

- 1045 (I) Schematic diagram and heatmap of real-time place aversion (RTPA) test with CGRP^{PBeI} cell body
1046 stimulation.
1047 (J) Time spent in the stimulated zone during the RTPA test with CGRP^{PBeI} cell body stimulation.
1048 (K) Representative image of optic fiber placement in the CeA (red dot).
1049 (L) Time spent in the stimulated zone during the RTPA test with CGRP^{PBeI→CeA} terminal stimulation.
1050 (M) Time spent freezing during the context test.
1051 (N) Time spent freezing during cue test after pairing optogenetic stimulation and tone for cued fear
1052 conditioning. Scale bars indicate 200 μ m.

1053

1054

1055 **Statistics**

1056 (C) Repeated measure two-way ANOVA showed significance in laser x group interaction ($F(1, 17) = 17.69$,
1057 $p = 0.0006$) and laser ($F(1, 17) = 20.19$, $p = 0.0003$) but not group ($F(1, 17) = 4.03$, $p = 0.0608$). Laser ON
1058 and OFF in Chr2 ($p < 0.0001$), and EYFP and Chr2 during ON ($p < 0.001$) had statistically significant
1059 difference with Sidak's multiple comparisons test.

1060 (E) Repeated measure two-way ANOVA showed significance in only laser x group interaction ($F(1, 18) =$
1061 8.718 , $p = 0.0085$) but not laser ($F(1, 18) = 3.159$, $p = 0.0924$) and group ($F(1, 18) = 4.343$, $p = 0.0517$).
1062 Laser ON vs OFF in Chr2 ($p < 0.05$), and EYFP vs Chr2 during ON ($p < 0.01$) have statistically significant
1063 difference with Sidak's multiple comparisons test.

1064 (F) EYFP: 3.842 ± 0.89 ($n = 13$), Chr2: 31.92 ± 7.806 ($n = 10$). Unpaired t test (two-tailed), $p = 0.0005$.

1065 (G) Repeated measure two-way ANOVA showed significance in CS x group interaction ($F(1, 21) = 12.41$,
1066 $p = 0.0020$), CS ($F(1, 21) = 38.26$, $p < 0.0001$) and group ($F(1, 21) = 8.392$, $p = 0.0086$). CS- vs CS+ in
1067 Chr2 ($p < 0.0001$), and EYFP vs Chr2 during CS+ ($p < 0.001$) have statistically significant difference
1068 with Sidak's multiple comparisons test.

1069 (J) Repeated measure two-way ANOVA showed significance in laser x group interaction ($F(1, 9) = 10.49$,
1070 $p = 0.0102$) and laser ($F(1, 9) = 8.959$, $p = 0.0151$) but not group ($F(1, 9) = 1.159$, $p = 0.3096$). Laser ON
1071 and OFF in Chr2 ($p < 0.01$), and EYFP and Chr2 during ON ($p < 0.05$) had statistically significant
1072 difference with Sidak's multiple comparisons test.

1073 (L) Repeated measure two-way ANOVA showed significance in laser x group interaction ($F(1, 9) = 12.91$,
1074 $p = 0.0058$) and laser ($F(1, 9) = 6.094$, $p = 0.0357$) but not in group ($F(1, 9) = 4.405$, $p = 0.0652$). Laser
1075 ON and OFF in Chr2 ($p < 0.01$), and EYFP and Chr2 during ON ($p < 0.01$) had statistically significant
1076 difference with Sidak's multiple comparisons test.

1077 (M) EYFP: 6.278 ± 1.244 ($n = 5$), Chr2: 28.93 ± 5.133 ($n = 6$). Unpaired t test (two-tailed), $p = 0.0035$.

1078 (N) Repeated measure two-way ANOVA showed significance in CS x group interaction ($F(1, 9) = 12.67$,
1079 $p = 0.0061$), CS ($F(1, 9) = 8.226$, $p = 0.0185$) and group ($F(1, 9) = 6.314$, $p = 0.0332$). CS- vs CS+ in
1080 Chr2 ($p < 0.01$), and EYFP vs Chr2 during CS+ ($p < 0.01$) have statistically significant difference with
1081 Sidak's multiple comparisons test.

1082

1083

1084

1085

1086

1087

1088

1089 **Supplementary Information**

1090

1091 **Materials and methods**

1092 **Animals**

1093 All protocols for animal experiments were approved by the IACUC of the Salk Institute for Biological
1094 Studies according to NIH guidelines for animal experimentation. The *Calca^{Cre}*, and *Tacr1^{Cre}* transgenic
1095 mouse lines used in this study were generated from the Richard Palmiter's laboratory (Han et al., 2015 or
1096 Carter et al., 2013) *Cdx2^{FlpO}* line was generated from the Martyn Goulding's laboratory. *Calca^{CreER}* mouse
1097 line was generated from the Pao-Tien Chuang's laboratory. RiboTag *Rpl22^{HA/HA}* (Stock No. 011029) and
1098 Ai65 (Stock No: 021875) mouse line was obtained from the Jackson Laboratory. All mouse lines are
1099 backcrossed with C57Bl/6J for > 6 generations. Male and female mice were used in all studies. Animals
1100 were randomized to experimental groups and no sex differences were noted. Mice were maintained on a
1101 normal 12 hours light/dark cycle and provided with food and water *ad libitum*.

1102

1103 ***Stereotaxic surgery for virus injection and optic fiber implantation***

1104 Mice were anesthetized by isoflurane gas anesthesia (induction at 3.5%, and maintenance at 1.5-2%, the
1105 Dräger Vapor® 2000; Draeger, Inc., USA). Mice were then placed on a stereotaxic frame (David Kopf
1106 Instruments, USA). Holes were drilled with a micromotor handpiece drill (Freedom, USA) after the
1107 exposure of the skull. The virus was injected using a syringe (65458-01, Hamilton, USA) connected to an
1108 ultra-micropump (UMP-3, World Precision Instruments, USA). Unilateral (right side) and bilateral
1109 injections were made for the following target regions: SPFP (antero-posterior (AP), -3.1 mm; medio-lateral
1110 (ML), 2.0 mm; dorso-ventral (DV) -3.6 mm from bregma) or PBel (AP, -5.1 mm; ML, 1.35 mm; DV, -3.5
1111 mm). Viruses were injected at a rate of 0.08 µl/min (total volume of 0.75 µl for optogenetic projection
1112 studies and 0.5 µl for all the others) and the syringe needle was slowly removed from the injection site
1113 seven-minute after injection. To determine the inputs to CGRP^{SPFP} and CGRP^{PBel} neurons, 0.5 µl of AAV8-
1114 hSyn-FLEX-TVA-P2A-GFP-2A-oG (Salk Institute viral vector core, USA) was injected into the SPFP or
1115 PBel of *Calca^{Cre}* transgenic mice. After three weeks, 0.5 µl of EnvA-ΔG-rabies-mCherry (Salk Institute
1116 viral vector core, USA) was injected, and the mice were sacrificed five days after the injection. To silence
1117 the CGRP^{SPFP} and CGRP^{PBel} neurons, 0.5 µl of AAV-DIO-TetTox-GFP or AAV-DIO-EYFP was injected
1118 into the SPFP or PBel of *Calca^{Cre}* transgenic mice, and experiments were performed two weeks after
1119 injection. For fiber photometry experiments, mice were injected with 0.5 µl of either AAV-DIO-GCaMP6m,
1120 AAV-DIO-GCaMP7s or AAV-DIO-EYFP into the SPFP or PBel of *Calca^{Cre}* mice. Stainless-steel mono
1121 fiberoptic cannulas (400 µm diameter, 0.37 NA, Doric Lenses) were implanted above the SPFP or PBel.
1122 For electrophysiology, mice were injected with 0.5 or 0.75 µl of AAV1-DIO-ChR2-EYFP into the SPFP or
1123 PBel of *Calca^{Cre}* mice. Experiments were performed two weeks after viral injection for recording SPFP and
1124 PBel neurons or four weeks after injection for recording cells in terminal regions. For optogenetics, mice
1125 were injected with 0.5 or 0.75 µl of AAV1-DIO-ChR2-EYFP or AAV-DIO-EYFP into the SPFP or PBel
1126 of *Calca^{Cre}* mice and custom made mono fiberoptic cannula (200 µm diameter, 0.22 NA) were implanted
1127 above SPFP (0.5 mm above the injection site), PBel (0.5 mm above the injection site), Astr (AP, -1.8 mm;
1128 ML, 3.3 mm, DV, -3.8 mm from bregma), lateral amygdala (LA; AP, -1.8 mm; ML, 3.6 mm, DV, -4.0 mm
1129 from bregma), pIC (AP, -1.5 mm; ML, 4.6 mm, DV, -3.0 mm from bregma) or central amygdala (CeA; AP,
1130 1.2 mm; ML, 2.7 mm; DV, -4.2 mm from bregma). Experiments were executed two weeks after injection
1131 to manipulate SPFP neurons or four weeks later for terminal stimulations.

1132

1133 ***Histology and quantification of rabies tracing experiment***

1134 Mice were intracardially perfused with 4% paraformaldehyde in PBS 5 days after the rabies virus injection.
1135 Spinal cords were post-fixed at 4°C for 1 hr and dehydrated with 30% sucrose at 4°C overnight. 40 µm
1136 transverse sections were obtained with a cryostat (CM 1950, Leica, USA) throughout the spinal cord. Spinal
1137 cord slices were directly dry mounted on superfrost plus microscope slide glasses (12-550-15, Fisher
1138 Scientific, USA). The labeled neurons were counted manually by dividing the transverse spinal sections
1139 into four groups (cervical, thoracic, lumbar, and sacral) or different dorsal horn layers. Brains were kept in
1140 4% PFA overnight for post-fixation and dehydrated in 30% sucrose for 1-2 days before sectioning. Frozen
1141 brains were cut into 50 µm coronal slices with a cryostat and stored in Phosphate buffered saline before
1142 mounting. Both spinal cord and brain tissues were mounted on a slide glass with a DAPI containing
1143 mounting solution (0100-20, SouthernBiotech, USA).

1144

1145 ***Fiber photometry***

1146 Bulk calcium signals from the CGRP^{SPFP} and CGRP^{PBeI} neurons were monitored using a custom-built fiber
1147 photometry system based on the open-source pyPhotometry platform
1148 (<https://pyphotometry.readthedocs.io/en/latest/>). 465 nm LED was used to induce Ca²⁺ dependent
1149 fluorescence signals, and 405 nm LED was used for Ca²⁺ independent (isosbestic) fluorescence signals.
1150 Motion corrected $\Delta F/F$ was calculated by a post-hoc analysis ($\Delta F/F = F_{465} - F_{405fit} / F_{405fit}$). The least-squares
1151 polynomial function was used to calculate F_{405fit} , and the area under the curve was used to analyze the data.

1152

1153 ***Multi-modal aversive stimuli experiments***

1154 ***Mechanical and thermal stimuli***

1155 Mechanical and thermal stimuli were applied to mice forepaw, hind paw, or tail. Mechanical pressure was
1156 applied using a dial tension gauge (ATG-300-1, Vetus Instruments, USA) with stimulus strength 0, 50, 100,
1157 200 g. The thermal stimulus was applied using a custom-made temperature-controlled hot-rod (TA4-
1158 SNR+K, Mypin, China) at 25, 35, 45, and 55°C. A stable baseline was recorded first for 10 s, and stimuli
1159 were applied immediately after 5 seconds.

1160 ***Formalin test***

1161 For fiber photometry, lightly anesthetized mice were placed in the stereotaxic frame head fixed to minimize
1162 movement. 10 µl of 4% formalin (1.6% Paraformaldehyde, 19210, Electron Microscopy Sciences, USA)
1163 was injected subcutaneously on the contralateral forepaw after at least 5 min of stable baseline. Calcium
1164 transients were recorded for 45 min. For the loss of function experiment, 10 µl of 4 % formalin was injected
1165 subcutaneously on one side of the forepaw. Mice were then placed in a Plexiglas chamber (10 x 10 x 13
1166 cm) with a mirror placed behind. Behaviors were recorded for an hour, and licking behaviors were manually
1167 counted throughout the experiment.

1168 ***Auditory and visual stimuli***

1169 For both auditory and visual stimuli experiments, mice were placed in a cylinder-shaped arena (11 cm
1170 diameter with 15 cm height) with homecage bedding and were habituated for 30-120 min. For auditory
1171 experiments, after a stable 10s baseline, an intense sound (85 dB, 2 s) or a control sound (70 dB) was played.
1172 For the loss-of-function experiments, mice were placed inside an open field chamber and were habituated
1173 for 10 min. After 1 min baseline, an intense sound (85 dB, 2 s) was delivered three times with an inter-
1174 stimulus interval of 28 s. All the trials were recorded by a USB camera (DFK 33GX236, Imagine Source,
1175 Germany) attached to a computer, and freezing behavior was analyzed using video-tracking software
1176 (Ethovision XT, Noldus, Netherlands). For visual looming experiments, after a stable 10 s baseline, an

1177 expanding looming stimulus (2 s) was delivered three times with 10s inter-stimulus interval with a LED
1178 screen facing the arena from above. For the loss-of-function experiment, mice were placed in a cage with
1179 bedding and were positioned under the same LED screen. Mice were habituated for 20-30 min. When mice
1180 were in the center, the expanding looming stimulus (2 s) was delivered three times with 10 s inter-stimulus
1181 interval. All the trials were recorded by a USB camera (DFK 33GX236, Imagine Source, Germany)
1182 attached to a computer, and freezing behavior was analyzed using video-tracking software (Ethovision XT,
1183 Noldus, Netherlands) with manual counting for the duration of tail rattling behaviors.

1184 *Gustatory stimulus*

1185 For fiber photometry, mice were placed in the same arena for auditory and visual stimulus experiments with
1186 an additional 2 cm drilled hole. The water bottle spout was inserted into the hole, and the calcium signal
1187 was measured when the mice were licking. The bottle was filled with water or quinine (0.5 mM, QU109,
1188 Spectrum Chemical, USA). For the loss-of-function experiment, mice were water-deprived overnight. The
1189 next day, mice were placed in a homecage with a water-, and 0.5 mM quinine-containing bottle inserted
1190 into the water valve slot. Mice were allowed to drink for 10 min without habituation. All the trials were
1191 recorded by a USB camera (DFK 33GX236, Imagine Source, Germany) attached to a computer, and the
1192 licking behaviors were counted manually.

1193 *Olfactory stimulus*

1194 For fiber photometry, mice were placed in the same arena for gustatory stimulus experiments. Water- or
1195 Trimethylthiazoline (TMT, 97%, 5 μ l, 1G-TMT-97, BioSRQ, USA)-soaked cotton swap was introduced
1196 into the hole. Calcium signals were measured when mice smelled the cotton swap. For the loss-of-function
1197 experiment, mice movement was tracked in a two-chamber arena (30 x 60 x 30 cm) with a USB camera
1198 (DFK 33GX236, Imagine Source, Germany) using video-tracking software (EthoVision XT 12, Noldus,
1199 Netherlands). Two Petri dishes with small holes were placed in each chamber (one at the corner of the left
1200 chamber, and the other to the corner of the right chamber). On day 1, mice were able to habituate and
1201 explore the arena for 10 min. The next day, a water-soaked cotton swap, or TMT-soaked cotton swap were
1202 placed in each dish. Mice were first placed at the center and monitored for 10 minutes as they interacted
1203 with the two dishes.

1204 *Foot shock*

1205 A fear-conditioning chamber (26 x 30 x 33 cm, ENV-007CT, MED Associates INC, USA) with a metal
1206 grid floor (ENV-005, MED Associates INC, USA) connected to a standalone aversive electric shock
1207 stimulator (ENV-414S, MED Associates INC, USA) was used for foot shock delivery. A USB camera
1208 (DFK 33GX236, Imagine Source, Germany) was connected to a computer, and the video tracking software
1209 (Ethovision XT, Noldus, Netherlands) was used for shock delivery and behavioral analysis. The chamber
1210 was enclosed in a light- and sound-attenuating cubicle (ENV-018MD, MED Associates INC, USA). The
1211 chamber was cleaned with 70% ethanol and double distilled water between each trial.

1212 For fiber photometry and the loss-of-function experiment, mice were placed inside the chamber without
1213 habituation. After 2 min of baseline, an electric shock (2 s, 0.6 mA) was delivered, and the behavior was
1214 recorded for an extra 2 min. Freezing behavior was monitored before (habituation), after (conditioning),
1215 and one day after (post-test) the shock.

1216 *Elevated plus maze test*

1217 A custom-built elevated plus maze with two transparent closed arms (77 x 7 x 30 cm) and two open arms
1218 (77 x 7 x 2 cm) was used to monitor the anxiety-like behaviors of test mice. This maze was elevated 70 cm
1219 above ground for all tests. Mice were placed to the tip of the open arm by facing towards the center of the
1220 maze. The behavior was video recorded for 10 min and tracked with a video-tracking software (EthoVision

1221 XT 12, Noldus, Netherlands). Both 70% ethanol solution and deionized water were used to clean the maze
1222 immediately after each trial.

1223 *Hot plate test*

1224 Mice were placed into a cylinder-shaped transparent Plexiglas chamber (11 cm diameter with 15 cm length)
1225 on a heated hot plate (48 or 55°C, PE34, IITC Life Science, USA). The latency of various pain responses
1226 (hind paw shake, lick, or jump) was measured manually.

1227 *Electronic von Frey test*

1228 A Dynamic Plantar Aesthesiometer (37450, Ugo Basile, Italy) was used to measure the mechanical pain
1229 thresholds. Mice were placed inside a Plexiglas chamber (10 x 10 x 13 cm) on a metal mesh floor and were
1230 habituated for 30 min. The max force of the system was set to reach 50 g at 20 s. The blunt metal rod of the
1231 aesthesiometer was placed under the hind paw and gradually protruded as the mice were immobile but
1232 awake. The latency and force delivered were automatically recorded as the mouse withdraw hind paw from
1233 the metal rod. The measurement was performed 5 times with 5-10 min intervals in between trials and
1234 averaged for a final mechanical threshold value.

1235

1236 ***Optogenetics***

1237 A 470 nm laser (LRD-0470-PFFD-00100-05, LaserGlow Tech., Canada) was used for all optogenetic
1238 experiments in this study. Optic fibers were bilaterally connected to pre-implanted optic ferrules on the
1239 mice. All mice were optogenetically stimulated 90 min before sacrifice for cFos immunohistochemistry.

1240 *Hot plate test*

1241 The experiments were performed as described in the '*Hot plate test*' section above with minor modification
1242 for optogenetic stimulation. The order of laser ON or OFF was counterbalanced, and the interval time
1243 between each experiment was more than 30 min.

1244 *Electronic von Frey test*

1245 The experiments were performed as described above in the '*Electronic von Frey test*' with minor
1246 modification for optogenetic stimulation. The laser was on immediately before the metal rod touched the
1247 paw pad and turned off right after paw withdrawal.

1248 *Real-time place aversion (RTPA)*

1249 A two-chamber arena (30 x 60 x 30) was used for the RTPA test. The behavior was tracked with a USB
1250 camera (DFK 33GX236, Imagine Source, Germany) using video-tracking software (EthoVision XT 12,
1251 Noldus, Netherlands). After connecting the optic fiber, mice were placed in one side of the chamber. No
1252 stimulation was given for 10 min baseline. Afterward, one side of the chamber was randomly selected, and
1253 the mouse was photostimulated (20 Hz for cell body stimulation, and 40 Hz for terminal stimulation, 8-9
1254 mW) for 20 min. The stimulated side was counterbalanced between animals. Mice showing over 15%
1255 preference to one side during baseline were excluded.

1256 *Context-dependent optogenetic conditioning*

1257 An open field arena (40 x 40 x 30 cm) was used for context-dependent threat conditioning. After 10-min
1258 habituation to head-attached optic fibers in the home cage, mice were placed in the novel open field area
1259 and received photostimulation (20 Hz, and 8-9 mW) throughout the experiment. After 24 h, the mouse was
1260 re-introduced in the same context to test whether the photo-stimulation produced aversive memory. All the
1261 trials were recorded by a USB camera (DFK 33GX236, Imagine Source, Germany) attached to a computer,
1262 and freezing behavior was analyzed by a video-tracking software (EthoVision XT 12, Noldus, Netherlands).

1263 *Auditory cue dependent optogenetic conditioning*

1264 The same fear-conditioning chamber and the settings as described in the '*Foot shock*' section above were
1265 used. Two speakers (AX210, Dell, USA) were placed beside the chamber for CS. On day 1, the test mouse
1266 was habituated with the conditioning chamber, which was cleaned with 70% ethanol and DW immediately
1267 after each test. During habituation, optic fibers were connected bilaterally to the optic ferrules on the
1268 mouse's head, and the CS+ (30 s, 3 kHz pure tone, 75 dB) was delivered to the test mouse six times with
1269 random inter-event intervals. On day 2, the test mouse was returned to the same context with optic fibers
1270 connected and received 10-s photostimulation (20 Hz frequency for cell body and 40Hz for terminal
1271 stimulation, 8-9 mW intensity) as the US, which was co-terminated with CS+ six times with random inter-
1272 event intervals. On day 3, the conditioned mouse without the optic fiber connected was returned to the same
1273 context for 2 min. On day 4, a conditioned mouse without the optic fiber connected was introduced to a
1274 new context (a glass cylinder wrapped with a non-transparent material), and the CS+ was delivered without
1275 the US. All the trials were recorded by a USB camera (DFK 33GX236, Imagine Source, Germany) attached
1276 to the computer, and freezing behavior was analyzed by a video-tracking software (EthoVision XT 12,
1277 Noldus, Netherlands).

1278

1279 ***Immunohistochemistry***

1280 Mice were perfused intracardially with 4 % PFA solution in PBS, and the brain was extracted. The brain
1281 was kept in 4 % PFA overnight for post-fixation and dehydrated in 30 % sucrose for 1-2 days before
1282 sectioning. Frozen brains were cut into 40 μ m coronal slices with a cryostat (CM 1950, Leica, USA) and
1283 washed with PBST (Phosphate buffered saline with 0.1 % Tween-20 (BP337-500, Fisher BioReagents,
1284 USA)). Initial blocking was performed by 1hr incubation with 3 % normal donkey serum (NDS, 017-000-
1285 121, Jackson ImmunoResearch Laboratories, Inc., USA). After another round of washing with PBST, the
1286 slices were incubated with anti-GFP (diluted 1:100 in 3% NDS, GFP-1020, Aves, USA), anti-fos (1:10000,
1287 rabbit polyclonal), anti-Nav1.7 (1:200, ASC-008, Alomone), anti-Cav2.1 (1:100, ACC-001, Alomone,
1288 Isreal), or anti-FAAH (1:250, 101600, Cayman, USA) antibody at 4 °C overnight. The next day, brain
1289 tissues were rinsed with PBST, then incubated with anti-rabbit Alexa Fluor® 647-secondary antibody (1:500,
1290 711-605-152, Jackson ImmunoResearch Laboratories, Inc., USA), and / or anti-chicken Alexa Fluor® 488-
1291 secondary antibody (1:500, Jackson ImmunoResearch Laboratories) for 1 hr. After washing these brain
1292 slices with PBS, they were mounted on slide glass (12-550-143, Fisher Scientific, USA) with DAPI
1293 containing mounting solution.

1294

1295 ***Preparation of acute brain slices and electrophysiology***

1296 Mice were anesthetized with isoflurane and perfused via the vascular system using ice-cold cutting solution
1297 (110.0 mM choline chloride, 25.0 mM NaHCO₃, 1.25 mM NaH₂PO₄, 2.5 mM KCl, 0.5 mM CaCl₂, 7.0 mM
1298 MgCl₂, 25.0 mM glucose, 5.0 mM ascorbic acid and 3.0 mM pyruvic acid, bubbled with 95 % O₂ and 5 %
1299 CO₂). After decapitation, brains were quickly removed and chilled in an ice-cold cutting solution. Coronal
1300 slices containing the SPFP, PBel (250 μ m) or the amygdaloid complex (300 μ m) were cut by using a Leica
1301 VT 1200S Vibratome (Leica Biosystems Inc.), and subsequently transferred to a storage chamber
1302 containing artificial cerebrospinal fluid (aCSF; 124 mM NaCl, 2.5 mM KCl, 26.2 mM NaHCO₃, 1.2 mM
1303 NaH₂PO₄, 13 mM glucose, 2 mM MgSO₄ and 2 mM CaCl₂, at 32 °C, pH 7.4, bubbled with 95 % O₂ and
1304 5 % CO₂). After at least 30 min recovery time, slices were transferred to room temperature (22–24 °C) for
1305 at least 60 min before use. Slices were transferred into the recording chamber, perfused with aCSF (flow
1306 rate around 2 ml/ min). The temperature of aCSF was held constant at 32 °C by TC-324C temperature
1307 controller (Warner Instruments). Since CGRP-positive neurons express EGFP under the *Calca* promoter,

1308 they were visualized under Scientifica Microscope equipped with epifluorescence illumination at 490 nm
1309 LED. The Astr, LA, and IC neurons were visualized under trans-illumination. Whole-Cell patch clamp was
1310 performed with Multiclamp 700B amplifiers (Molecular Devices). Signals were digitized at 10 kHz with
1311 Digidata 1550B (Molecular Devices). For evoked EPSCs, synaptic responses were evoked with a broken
1312 glass pipette positioned 100 μm away from the recording glass electrode (3.0~5.0 M Ω , back filled with
1313 internal solution: CsMeSO₃ 130 mM, CsCl 5, HEPES 10 mM, MgCl₂ 2.5 mM, EGTA 0.6 mM, Sodium
1314 phosphocreatine 10 mM, Na₂ATP 4 mM and Na₃GTP 0.4 mM, pH 7.23, 285 Osm). The stimulus was given
1315 at 0.1 Hz. AMPA EPSC was recorded holding at -70 mV for 10 to 30 sweeps to get a stable response.
1316 NMDA EPSC was recorded at +40 mV for 10 – 15 sweeps. To ensure that the EPSCs were stable, the
1317 holding potential was set to -70 mV to check the AMPA EPSC change after NMDA EPSC recording.
1318 Evoked EPSCs were recorded with picrotoxin (100 μM) in the aCSF. mEPSCs were recorded in the
1319 presence of tetrodotoxin (1 μM) and picrotoxin (100 μM). To record optogenetically evoked EPSC and
1320 IPSC, slices were harvested from the AAV-DIO-ChR2-EYFP injected *Calca*^{Cre} mice brain. 2-ms 470 nm
1321 LED light (TTL from Clampex to Cool Led pE-300) was illuminated through 40X NA 0.8 objective lens
1322 at 0.1 Hz to evoke optogenetically evoked postsynaptic current. The internal solution was calculated to
1323 make chloride reversal potential at -70 mV. EPSCs were recorded at -70 mV, and IPSCs were recorded at
1324 0mV. CNQX (10 μM) was perfused to check the glutamatergic synapse. EPSCs and IPSCs were analyzed
1325 using pCLAMP 10 software (Molecular Devices). NMDA EPSCs were defined as signals 100 ms apart
1326 from stimulus artifacts. mEPSCs were analyzed using Mini Analysis Program (Synaptosoft).

1327

1328 **Imaging**

1329 The images were taken with an automatic fluorescence microscope (BZ-X710, Keyence, USA) using
1330 included imaging software (BZ-X viewer, Keyence, USA) or with a scanning confocal microscope (FV
1331 1000, Olympus, Japan) using with Fluoview software (Olympus, Japan). For quantification purposes,
1332 images were processed with the same gain, offset, and exposure time. Cell counting for retrograde tracing
1333 was done manually.

1334

1335 **RiboTag Transcriptomic Profiling**

1336 To label the active transcriptome of CGRP^{SPFP} and CGRP^{PBel} neurons, we crossed *Calca*^{CreER} with RiboTag
1337 *Rpl22*^{HA/HA} mice. To induce gene expression, 200 μl of tamoxifen freshly prepared with 20 mg/ml in corn
1338 oil and dissolved overnight with continuous agitation was administered intraperitoneally for five
1339 consecutive days in each mouse. Experiments were performed two weeks after the final tamoxifen injection.
1340 250 μm thick slices containing the PBel and the SPFP were obtained using a VT 1200S Vibratome (Leica,
1341 Germany). The region of interest was further dissected using surgical scissors under the stereoscope.
1342 Tissues of interest from four *Calca*^{CreER}; RiboTag crossed mice (10-12 weeks old) were collected into 1.5
1343 mL microcentrifuge tubes containing homogenization buffer and were mechanically dissociated and lysed
1344 using pellet pestles (Cat.no.7495211500-DS, DWK Life Sciences LLC, USA). Total RNA was extracted
1345 from 15% of cleared lysate for input samples. The remaining lysate was incubated with mouse anti-HA
1346 antibody (Cat.no.MMS-101R, Biolegend, USA) and was rocked for 4 hours at 4 °C. Afterward, magnetic
1347 beads (Cat.no.88803, Thermo Fisher Scientific, USA) were added, and the solution was incubated overnight,
1348 rocking at 4 °C. The beads were washed three times in high salt solution. The bound ribosomes and RNA
1349 were separated from the beads by 30 s of vortexing in RLT lysis buffer as IP. All RNA samples were
1350 purified from the IP and corresponding input samples (Qiagen RNeasy Mini Kit, cat.no. 74104), then
1351 quantified with the Qubit RNA Assay Kit (Invitrogen, USA) and analyzed with the RNA 6000 Pico Kit

1352 (Agilent, USA). Isolated RNA was prepared using the Trio RNA-Seq (Cat. No. 0507-08; NuGEN, USA).
1353 Briefly, cDNA was synthesized from the total RNA using reverse transcriptase with oligo dT and
1354 resynthesized to produce double-stranded cDNA. After amplifying double-stranded cDNA, cDNA was
1355 purified with AMPure XP Beads (Cat. No. A63881; Beckman Coulter, USA), fragmented to the library,
1356 and classified using a barcoded adaptor. All libraries were quantified by qPCR and analyzed with the RNA
1357 6000 Pico Kit. RNA library quality was checked using the 2100 Bioanalyzer (Agilent, USA). Barcoded
1358 samples were pooled and sequenced on the NextSeq500 (Illumina, USA) with the 75 bp read length single-
1359 end. Image analysis and base calling were conducted using the Illumina CASAVA-1.8.2 software. The
1360 FastQC package was utilized to evaluate the sequencing read quality. Fastq reads were then aligned to the
1361 reference genome (GRCm38.p6) using the STAR tool (version 2.7.2) in a pair-end mode. The quantification
1362 package RSEM (version 1.2.28) was employed to calculate gene expression from BAM files using the
1363 default setting changed to pair-end mode. In doing so, estimated count and TPM (Transcripts Per Million)
1364 were generated. Fold changes were calculated from TPM values (estimated counts, > 20) between HA-tag
1365 and HA negative controls., The ggplot2 package from R was utilized to visualize fold changes. UP (> 2.5
1366 fold change) and DOWN (< - 2.5 fold change) were highlighted with orange and blue colors, respectively.

1367

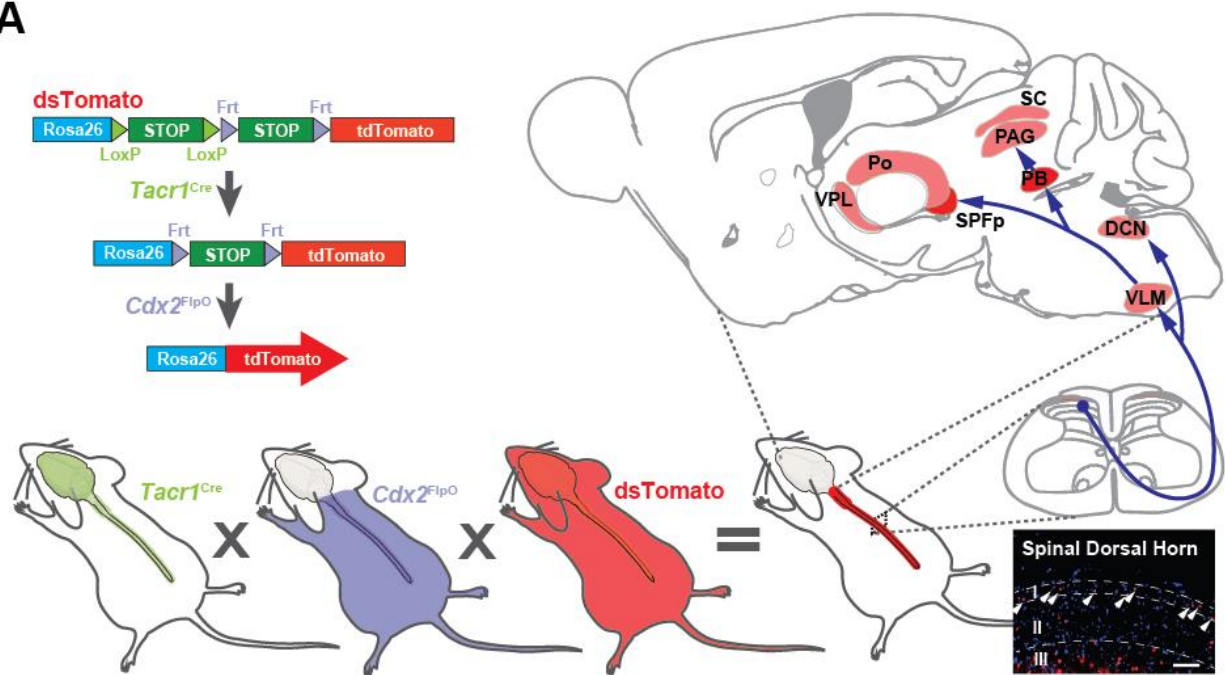
1368 *Statistical analysis*

1369 All data are shown as mean \pm s.e.m. and analyzed using Student's t-test, one-way ANOVA with Tukey's
1370 post hoc comparison, and two-way ANOVA with Sidak's post hoc comparison. All the statistical analyses
1371 were done using Prism 6 (GraphPad Software Inc., USA). NS $p > 0.05$, * $p < 0.05$, ** $p < 0.01$, *** $p <$
1372 0.001

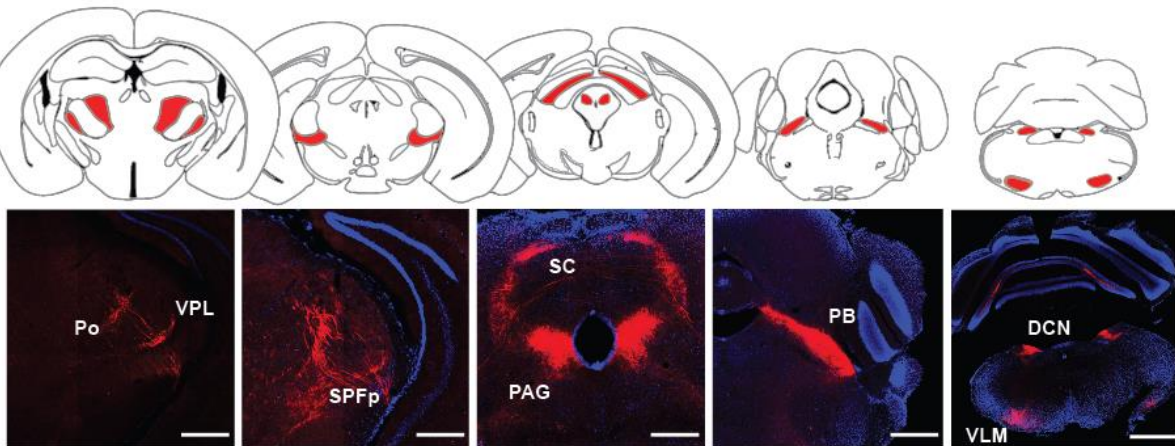
1373

1374 **Supplementary Figure Legends**

A



B

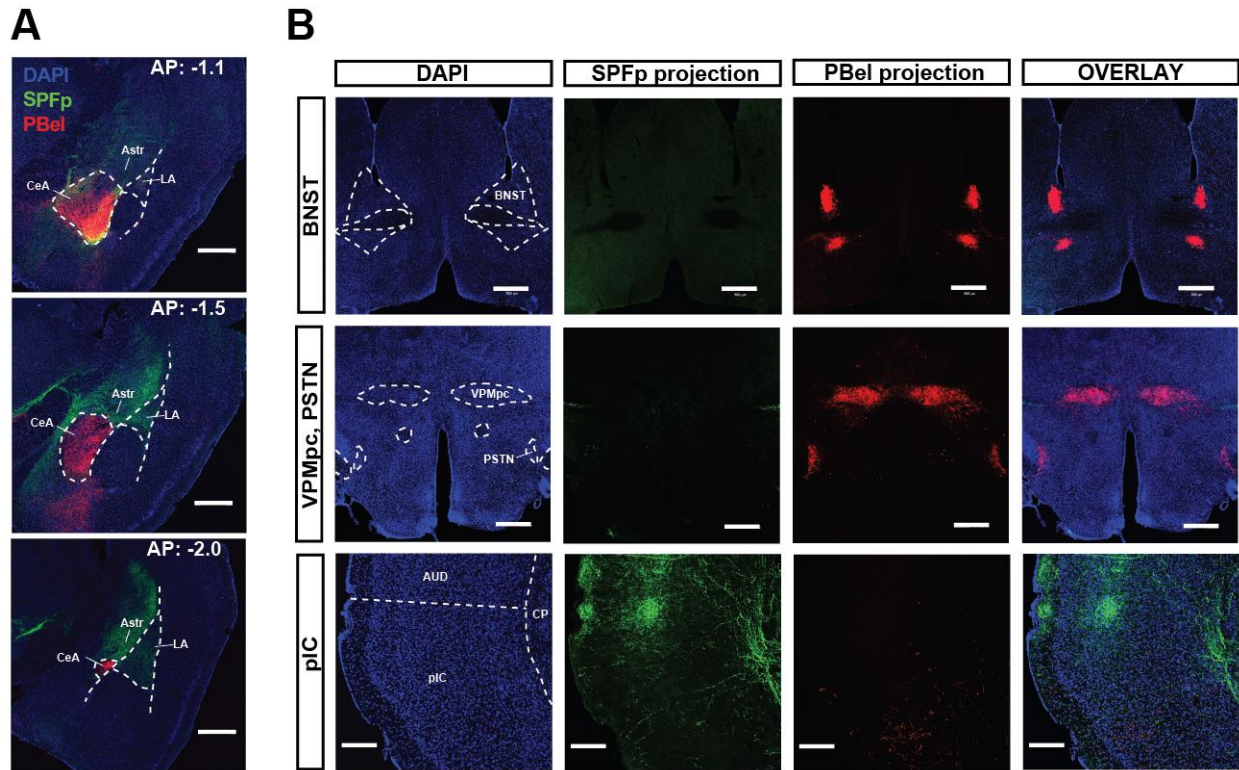


1375 **Figure S1. Identification of direct spino-recipient areas in the brain by specific genetic labeling of**
 1376 ***Tacr1*-positive spinal projection neurons.**
 1377

1378 (A) Schematics of the triple cross strategy to specifically label *Tacr1*-expressing neurons in the spinal dorsal
 1379 horn. Scale bar indicates 200 μ m.

1380 (B) Spinal *Tacr1*-expressing neurons send projections to the posterior complex of the thalamus (PO),
 1381 ventral posterolateral nucleus of the thalamus (VPL), the ventral posteromedial nucleus of the thalamus
 1382 (VPM), SPFP, superior colliculus (SC), periductal gray (PAG), PB, dorsal column nuclei (DCN) and
 1383 ventrolateral medulla (VLM). Scale bar indicates 500 μ m.

1384



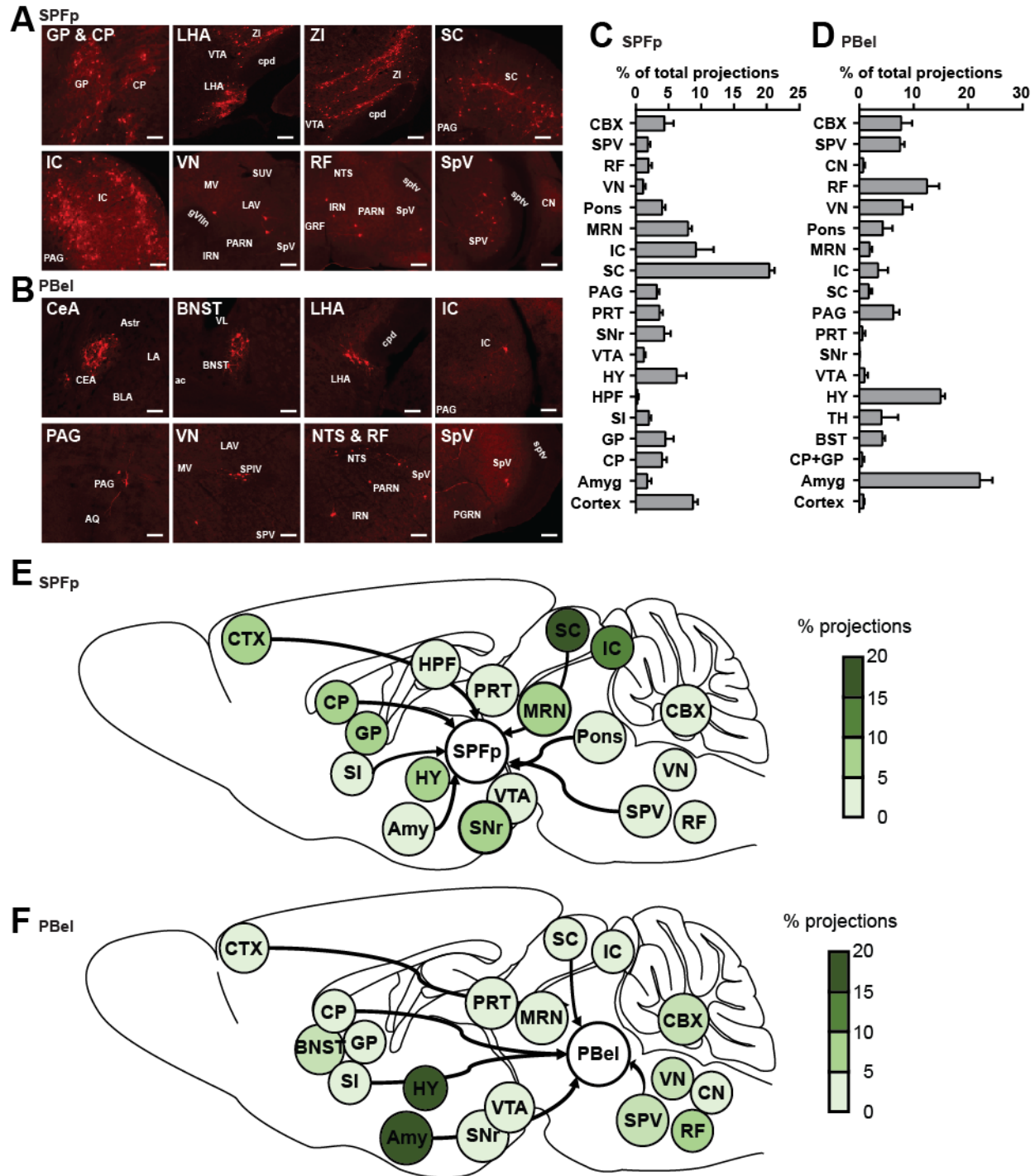
1385

1386 **Figure S2. Projections from CGRP^{SPFP} and CGRP^{PBel} neurons.**

1387 (A) Additional images from Figure 1A, B. Projections are prominent in the amygdala regions and have
1388 distinct patterns along the anterior-posterior axis; AP: -1.1, -1.5 and -2.0 mm from bregma. Scale bar
1389 indicates 500 μ m.

1390 (B) The CGRP^{PBel} neurons also project to BNST, VPMpc, PSTN, and ventral pIC. The CGRP^{SPFP} neurons
1391 project to the auditory cortex, and dorsal pIC. Scale bars indicate 500 μ m for BNST, and VPMpc; 200 μ m
1392 for pIC.

1393



1394

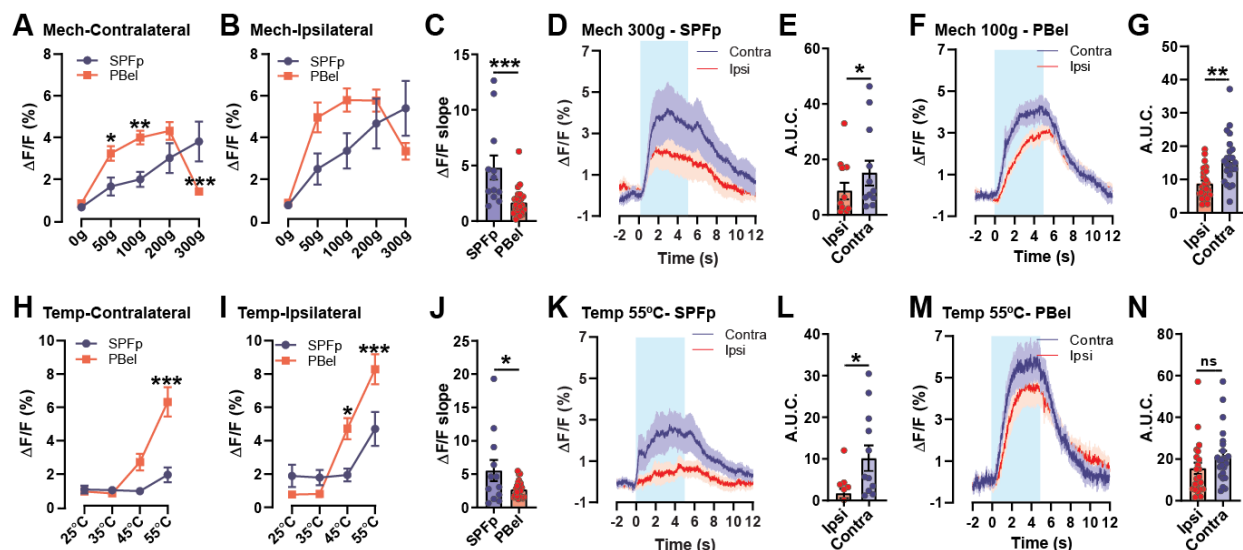
1395 **Figure S3. Retrograde tracing from $CGRP^{SPFp}$ and $CGRP^{PBeI}$ neurons.**

1396 (A, B) Example schematic of brain regions that send inputs to (A) $CGRP^{SPFp}$ and (B) $CGRP^{PBeI}$ neurons.
1397 Scale bars indicate 100 μ m.

1398 (C) Percentage of total projections from brain regions to $CGRP^{SPFp}$ neurons. These neurons receive input
1399 primarily from the cortex (auditory cortex, somatosensory cortex, motor cortex) and midbrain regions (SC,
1400 IC, MRN).

1401 (D) Percentage of total projections from brain regions to CGRP^{PBeI} neurons. These neurons receive input
1402 primarily from the amygdala (Amy, particularly the central amygdala), hypothalamus (HY, particularly the
1403 lateral hypothalamus, zona inserta, subthalamic nucleus, and parasubthalamic nucleus), and the medulla
1404 (including VN, RN, SpV).

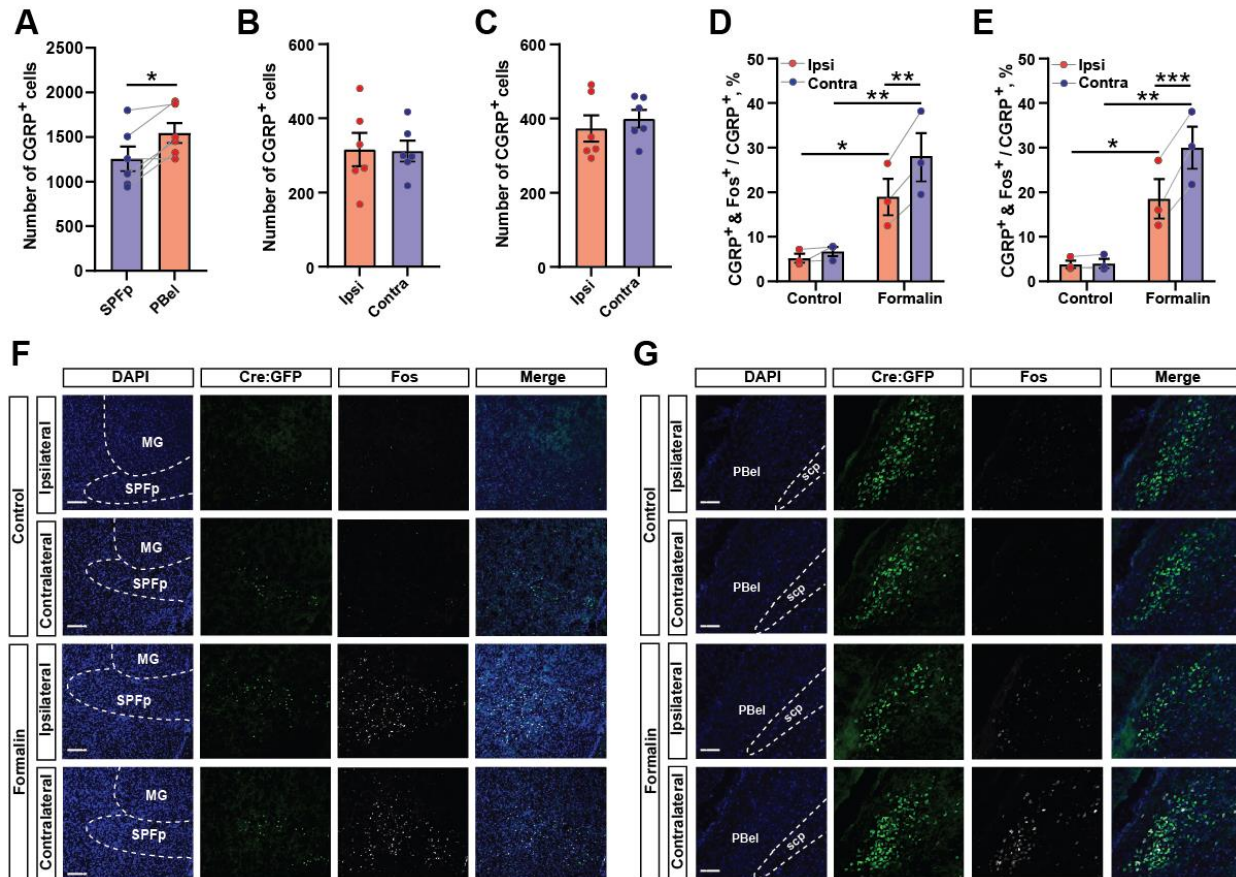
1405 (E, F) Diagram of the projection (%) from other brain regions to (E) CGRP^{SPFp} and (F) CGRP^{PBeI} neurons.
1406 CTX: cortex, Amy: amygdala, CP: striatum, GP: globus pallidus, BNST: bed nuclei of the stria terminalis,
1407 SI: substantia innominate, HPF: hippocampus, HY: hypothalamus, TH: thalamus, VTA: ventral tegmental
1408 area, SNr: substantia nigra, PRT: pretectal region, PAG: periaqueductal gray, SC: superior colliculus, IC:
1409 inferior colliculus, MRN: midbrain reticular nucleus, Pons: including the nucleus of the lateral lemniscus,
1410 pontine central gray, PBN, pontine reticular nucleus, VN: vestibular nucleus, RF: reticular formation, SpV:
1411 trigeminal spinal nucleus, CBX: cerebellum.
1412



1413
 1414 **Figure S4. CGRP^{SPFP} and CGRP^{PBel} neurons show lateralization to painful stimuli.**
 1415 (A, B) Maximum calcium responses of the CGRP^{SPFP} and CGRP^{PBel} neurons to (A) ipsilateral and (B)
 1416 contralateral mechanical stimulation.
 1417 (C) CGRP^{SPFP} displayed faster increase of the calcium responses (bigger initial slope) to the contralateral
 1418 mechanical stimulation (300g for CGRP^{SPFP} and 100g for CGRP^{PBel} neurons).
 1419 (D-G) Calcium responses of (D, E) CGRP^{SPFP} neurons by ipsilateral or contralateral 300g stimulation and
 1420 (F, G) CGRP^{PBel} neurons by 100 g stimulation.
 1421 (H, I) Maximum calcium responses of the CGRP^{SPFP} and CGRP^{PBel} neurons to (H) ipsilateral and (I)
 1422 contralateral thermal stimulation.
 1423 (J) Comparison of the initial slope of both neurons to contralateral 55 °C stimulation.
 1424 (K-N) Calcium responses of (K, L) CGRP^{SPFP} neurons and (M, N) CGRP^{PBel} neurons by ipsilateral or
 1425 contralateral 55 °C stimulation.

1426
 1427
 1428 **Statistics**
 1429 (A) Repeated measure two-way ANOVA showed significance in intensity X region interaction ($F(4, 136)$
 1430 $= 11.80$, $p < 0.0001$), intensity ($F(4, 136) = 17.66$, $p < 0.0001$), but not in region ($F(1, 34) = 2.075$, $p =$
 1431 0.1589). SPFP and PBel were significantly different in 50 ($p < 0.05$), 100 ($p < 0.01$) and 300 g ($p < 0.001$)
 1432 with Sidak's multiple comparisons test.
 1433 (B) Repeated measure two-way ANOVA showed significance in intensity X region interaction ($F(4, 136)$
 1434 $= 5.468$, $p = 0.0004$), intensity ($F(4, 136) = 18.46$, $p < 0.0001$), but not in region ($F(1, 34) = 1.528$, $p =$
 1435 0.2249).
 1436 (C) SPFP: 4.82 ± 1.08 ($n = 6$ mice, 12 trial), PBel: 1.68 ± 0.26 ($n = 6$ mice, 24 trial). Unpaired t test (two-
 1437 tailed), $p = 0.0007$.
 1438 (E) SPFP; Ipsi: 8.51 ± 3.00 ($n = 6$ mice, 12 trial), Contra: 15.06 ± 4.51 ($n = 6$ mice, 12 trial). Paired t-test
 1439 (two-tailed), $p = 0.0498$.
 1440 (G) PBel; Ipsi: 8.79 ± 0.95 ($n = 6$ mice, 24 trial), Contra: 15.26 ± 1.61 ($n = 6$ mice, 24 trial). Paired t-test
 1441 (two-tailed), $p = 0.0012$.

1442 (H) Repeated measure two-way ANOVA showed significance in intensity X region interaction ($F(3, 102)$
1443 = 8.995, $p < 0.0001$), intensity ($F(3, 102) = 17.79$, $p < 0.0001$), and region ($F(1, 34) = 11.19$, $p = 0.002$).
1444 SPFP and PBel were significantly different in 55 °C ($p < 0.0001$) with Sidak's multiple comparisons test.
1445 (I) Repeated measure two-way ANOVA showed significance in intensity X region interaction ($F(3, 102) =$
1446 10.16, $p < 0.0001$), intensity ($F(3, 102) = 40.99$, $p < 0.0001$), but not in region ($F(1, 34) = 2.885$, $p = 0.0986$).
1447 SPFP and PBel were significantly different in 45 ($p < 0.05$) and 55 °C ($p < 0.0001$) with Sidak's multiple
1448 comparisons test.
1449 (J) SPFP: 5.55 ± 1.59 ($n = 6$ mice, 12 trial), PBel: 2.72 ± 0.26 ($n = 6$ mice, 24 trial). Unpaired t test (two-
1450 tailed), $p = 0.0210$.
1451 (L) SPFP; Ipsi: 1.74 ± 1.12 ($n = 6$ mice, 12 trial), Contra: 10.15 ± 3.08 ($n = 6$ mice, 12 trial). Paired t-test
1452 (two-tailed), $p = 0.0146$.
1453 (N) PBel; Ipsi: 15.55 ± 2.71 ($n = 6$ mice, 24 trial), Contra: 21.24 ± 2.63 ($n = 6$ mice, 24 trial). Paired t-test
1454 (two-tailed), $p = 0.1385$.
1455



1456

1457

Figure S5. CGRP^{SPFP} and CGRP^{PBEl} are activated by formalin.

1458 (A) Number of CGRP positive cells in the SPFP and PBEl.

1459 (B, C) The number of CGRP positive cells in each side of the (B) SPFP and (C) PBEl.

1460 (D, E) The percentage of CGRP neurons co-expressing c-Fos in the (D) SPFP and (E) PBEl.

1461 (F, G) Representative images of the (F) SPFP and (G) PBEl. Scale bars indicate 200 μ m.

1462

1463

1464

Statistics

1465 (A) SPFP: 1255 ± 137.5 , PBEl 1545 ± 112.2 (n = 6 mice). Paired t-test (two-tailed), p = 0.0188.

1466 (B) SPFP; Ipsi: 315.5 ± 44.94 , Contra: 311.8 ± 27.85 (n = 6 mice). Paired t-test (two-tailed), p = 0.9057.

1467 (C) PBEl; Ipsi: 373.0 ± 35.34 , Contra 399.3 ± 24.06 (n = 6 mice). Paired t-test (two-tailed), p = 0.2958.

1468 (D) SPFP; Repeated measure two-way ANOVA showed significance in treatment X side interaction (F(1,

1469 4) = 17.42, p = 0.0140), treatment (F(1, 4) = 13.28, p = 0.0219), and side (F(1, 4) = 33.97, p = 0.0043).

1470 Ipsi vs contra was significant in formalin group (p < 0.01). Control vs formalin was significantly different

1471 in both ipsi (p < 0.05) and contra (p < 0.01) with Sidak's multiple comparisons test.

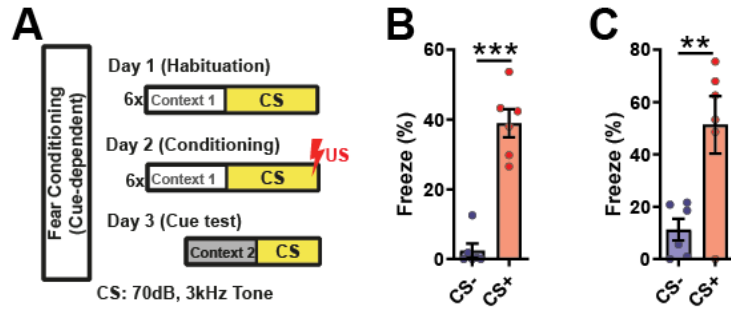
1472 (E) PBEl; Repeated measure two-way ANOVA showed significance in treatment X side interaction (F(1,

1473 4) = 55.27, p = 0.0017), treatment (F(1, 4) = 19.57, p = 0.0115), and side (F(1, 4) = 58.66, p = 0.0016).

1474 Ipsi vs contra was significant in formalin group (p < 0.001). Control vs formalin was significantly different

1475 in both ipsi (p < 0.05) and contra (p < 0.01) with Sidak's multiple comparisons test.

1476



1477

1478 **Figure S6. Cued fear conditioning with mice for CGRP^{SPFP} and CGRP^{PBel} fiber photometry.**

1479 (A) Behavioral scheme for cued fear conditioning. Low intensity (70 dB, 3kHz) tone was used as CS in
1480 order not to induce calcium activity by sound.

1481 (B, C) Freezing was induced in both (B) CGRP^{SPFP} and (C) CGRP^{PBel} group.

1482

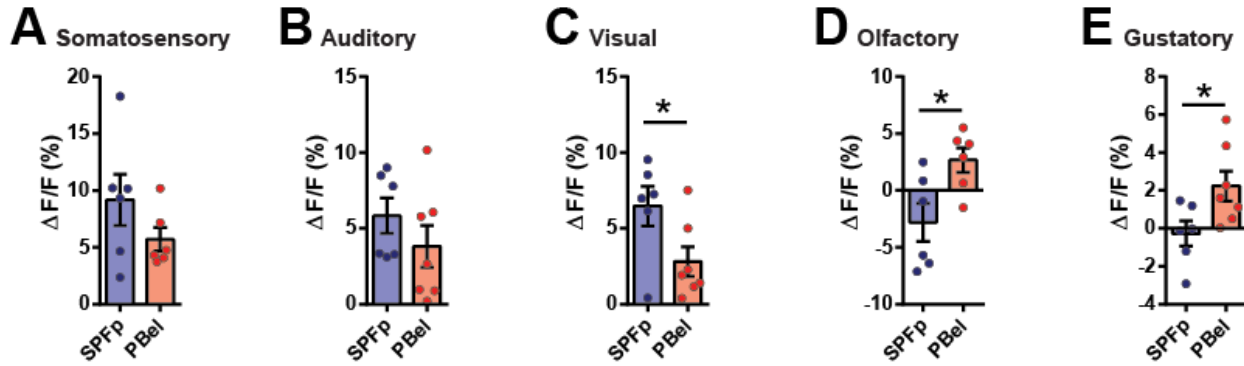
1483

1484 **Statistics**

1485 (B) SPFP; CS-: 2.47 ± 2.04 %, CS+: 38.96 ± 4.02 % (n = 6). Paired t test (two-tailed), $p < 0.0001$.

1486 (C) PBel; CS-: 11.27 ± 4.14 %, CS+ 51.31 ± 11.00 % (n = 6). Paired t test (two-tailed), $p = 0.01$.

1487



1488

1489 **Figure S7. The CGRP^{SPFp} and CGRP^{PBel} neurons are differentially activated by multiple sensory**
 1490 **threat cues.**

1491 (A) Calcium response in the CGRP^{SPFp} and CGRP^{PBel} neurons by 2-s electric foot shock (0.6 mA).

1492 (B) Calcium response in the CGRP^{SPFp} and CGRP^{PBel} neurons by 85-dB intense sound.

1493 (C) Calcium response in the CGRP^{SPFp} and CGRP^{PBel} neurons by rapidly expanding looming disk.

1494 (D) Calcium response in the CGRP^{SPFp} and CGRP^{PBel} neurons by TMT.

1495 (E) Calcium response in the CGRP^{SPFp} and CGRP^{PBel} neurons by 0.5 mM quinine solution.

1496

1497

1498 **Statistics**

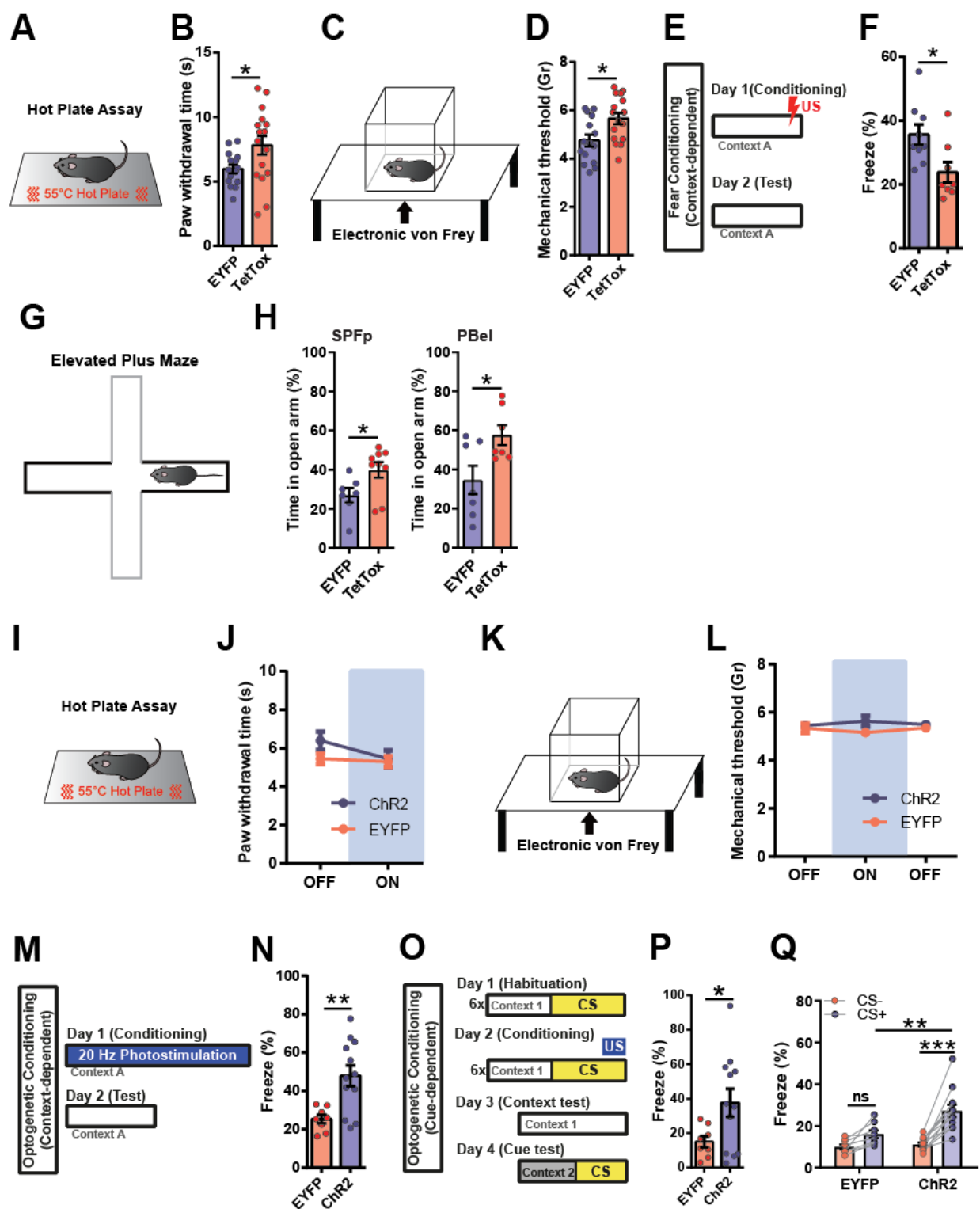
1499 (A) SPFp: $9.17 \pm 2.25\%$ (n = 6), PBel: $5.70 \pm 1.03\%$ (n = 6). Unpaired t test (two-tailed), p = 0.1917.

1500 (B) SPFp: $5.84 \pm 1.17\%$ (n = 6), PBel: $3.82 \pm 1.39\%$ (n = 7). Unpaired t test (two-tailed), p = 0.2987.

1501 (C) SPFp: $6.48 \pm 1.31\%$ (n = 6), PBel: $2.81 \pm 0.96\%$ (n = 7). Unpaired t test (two-tailed), p = 0.0418.

1502 (D) SPFp: $-2.80 \pm 1.68\%$ (n = 6), PBel: $2.68 \pm 1.07\%$ (n = 6). Unpaired t test (two-tailed), p = 0.0206.

1503 (E) SPFp: $-0.27 \pm 0.66\%$ (n = 6), PBel: $2.24 \pm 0.79\%$ (n = 7). Unpaired t test (two-tailed), p = 0.0363.



1504

1505 **Figure S8. Manipulation of CGRP^{SPFP} neurons in behavior assays.**

1506 (A, and B) Hot plate assay (55 °C) with CGRP^{SPFP} silenced mice.

1507 (C, and D) Automatic von Frey assay with CGRP^{SPFP} silenced mice.

1508 (E) Experimental design for contextual fear conditioning.

1509 (F) Quantification of freezing 24 hr after contextual fear conditioning.

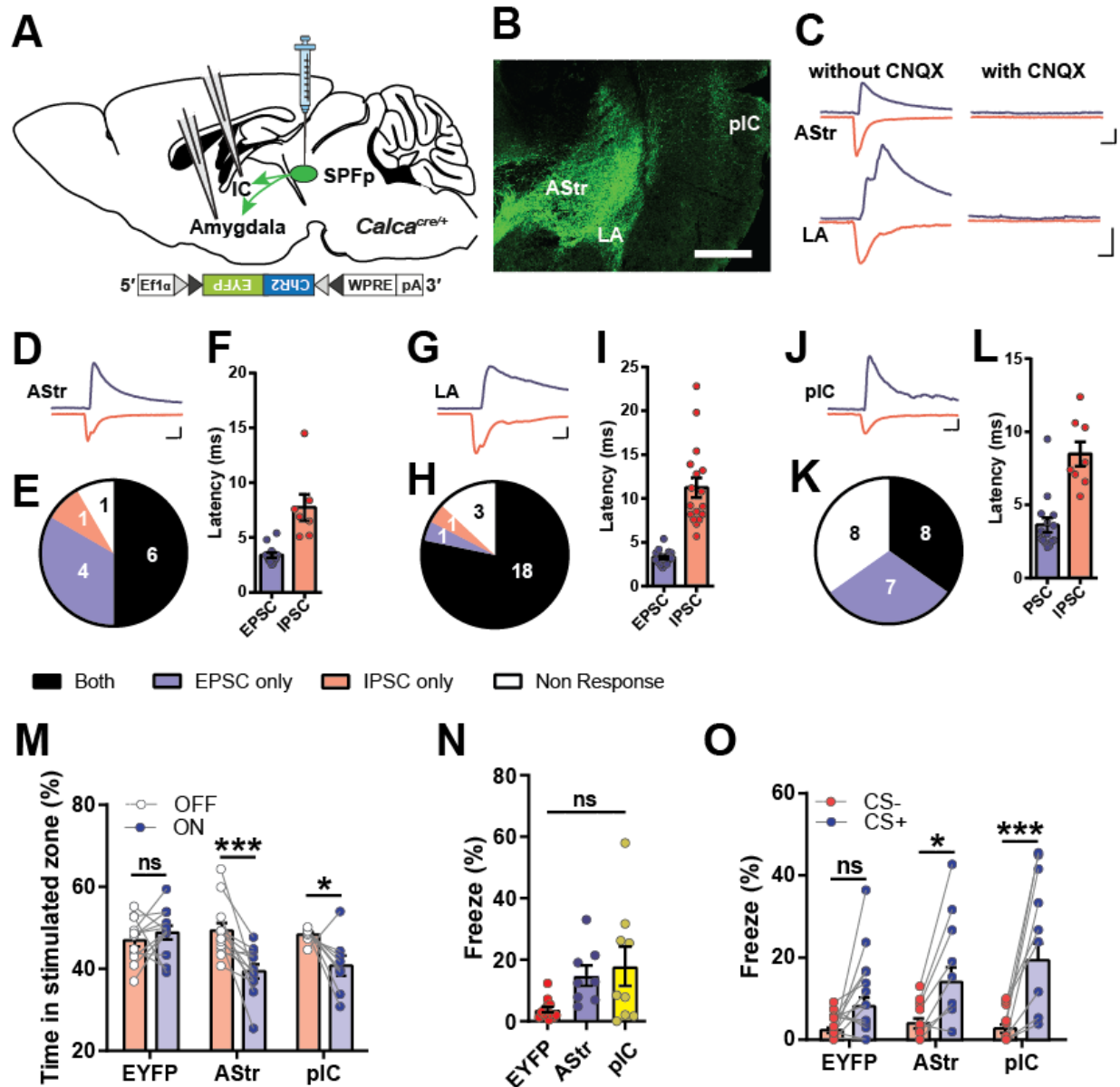
- 1510 (G) Schematic diagram of the elevated plus maze (EPM) test.
1511 (H) The EPM tests in CGRP^{SPFP} (left panel)- or CGRP^{PBel} neurons (right panel)-silenced mice.
1512 (I, and J) Optogenetic stimulation during hot plate assay (55 °C).
1513 (K, and L) Optogenetic stimulation during electric von Frey assay.
1514 (M) Schematic diagram of optogenetic fear conditioning (photostimulation was used instead of foot shock).
1515 (N) Quantified freezing level 24 hr after optogenetic conditioning.
1516 (O) Schematic diagram of optogenetic cue-dependent fear conditioning (photostimulation paired with 3
1517 kHz tone).
1518 (P) Context-dependent freezing 24 hr after optogenetic conditioning.
1519 (Q) Cue-dependent freezing 24 hr after optogenetic conditioning.

1520

1521

1522 **Statistics**

- 1523 (B) EYFP: 5.95 ± 0.33 s (n = 15), TetTox: 7.82 ± 0.73 s (n = 16). Unpaired t test (two-tailed), p = 0.0306
1524 (D) EYFP: 4.75 ± 0.24 g (n = 15), TetTox: 5.66 ± 0.33 g (n = 16). Unpaired t test (two-tailed), p = 0.0113
1525 (F) EYFP: 35.61 ± 3.18 % (n = 9), TetTox: 23.84 ± 3.17 % (n = 8). Unpaired t test (two-tailed), p = 0.0196
1526 (H) SPFP; EYFP: 26.96 ± 3.66 % (n = 7), TetTox: 39.83 ± 4.05 % (n = 9). Unpaired t test (two-tailed), p =
1527 0.0383.
1528 PBel; EYFP: 34.56 ± 7.37 % (n = 7), TetTox: 57.58 ± 5.15 % (n = 7). Unpaired t test (two-tailed), p =
1529 0.0250.
1530 (I) Repeated measure two-way ANOVA showed no significance in interaction (F (1, 16) = 1.79, p =
1531 0.2002), Laser (F (1, 16) = 3.36, p = 0.0857) and group (F (1, 16) = 1.49, p = 0.2393).
1532 (L) Repeated measure two-way ANOVA showed no significance in interaction (F (2, 36) = 1.72, p =
1533 0.1938), Laser (F (2, 36) = 0.06, p = 0.9465) and group (F (1, 18) = 1.26, p = 0.2768).
1534 (N) EYFP: 25.31 ± 2.18 % (n = 8), ChR2: 47.95 ± 5.42 % (n = 12). Unpaired t test (two-tailed), p = 0.0042.
1535 (P) EYFP: 15.06 ± 3.20 (n = 8), ChR2: 37.55 ± 8.13 (n = 12). Unpaired t test (two-tailed), p = 0.044.
1536 (Q) Repeated measure two-way ANOVA showed significance in CS x group interaction (F (1, 18) = 8.072,
1537 p = 0.0108), CS (F (1, 18) = 39.57, p < 0.0001) and group (F (1, 18) = 6.827, p = 0.0176). Freezing at CS-
1538 and CS+ in ChR2 group (p < 0.0001) and CS+ in EYFP and ChR2 (p < 0.01) were significantly different
1539 with Sidak's multiple comparisons test.



1540

1541

1542

1543

1544

1545

1546

1547

1548

1549

1550

1551

1552

1553

Figure S9. Mapping the functional downstream of CGRP^{SPFp} projection.

(A) Schematics of the experiment.

(B) Representative image of the projection regions from CGRP^{SPFp} neurons. Scale bar indicates 500 μ m.

(C) Example traces of an optically induced EPSC (blue) and IPSC (red) of AStr and LA without or with CNQX to confirm glutamatergic synapse. Scale bars indicate 10 ms and 50 pA.

(D) Examples of AStr EPSC (blue) and IPSC (red) traces by optogenetic terminal activation. Scale bars indicate 10 ms and 50 pA.

(E) Proportion of AStr cells with 'Both' EPSC and IPSC, 'EPSC only', 'IPSC only', or 'No-Response'.

(F) Onset of each AStr EPSC and IPSC to optogenetic stimulation.

(G-L) Results of the same experiments with (G-I) LA and (J-L) pIC neurons. Scale bars indicate 10 ms and 50 pA.

(M) Result of RTPA with terminal photo-stimulation.

(N) Context-dependent freezing at 24 hr after terminal photo-stimulation conditioning.

1554 (O) Cue-dependent freezing at 24 hr after terminal photo-stimulation conditioning.

1555

1556

1557 **Statistics**

1558 (F) Astr; EPSC: 3.40 ± 0.25 ms (n = 12 cells), Astr IPSC: 7.74 ± 1.21 ms (n = 7 cells). Unpaired t test (two-
1559 tailed), p = 0.0003.

1560 (I) LA; EPSC: 3.30 ± 0.16 ms (n = 21 cells), LA IPSC: 11.24 ± 1.13 ms (n = 17 cells). Unpaired t test (two-
1561 tailed), p < 0.0001.

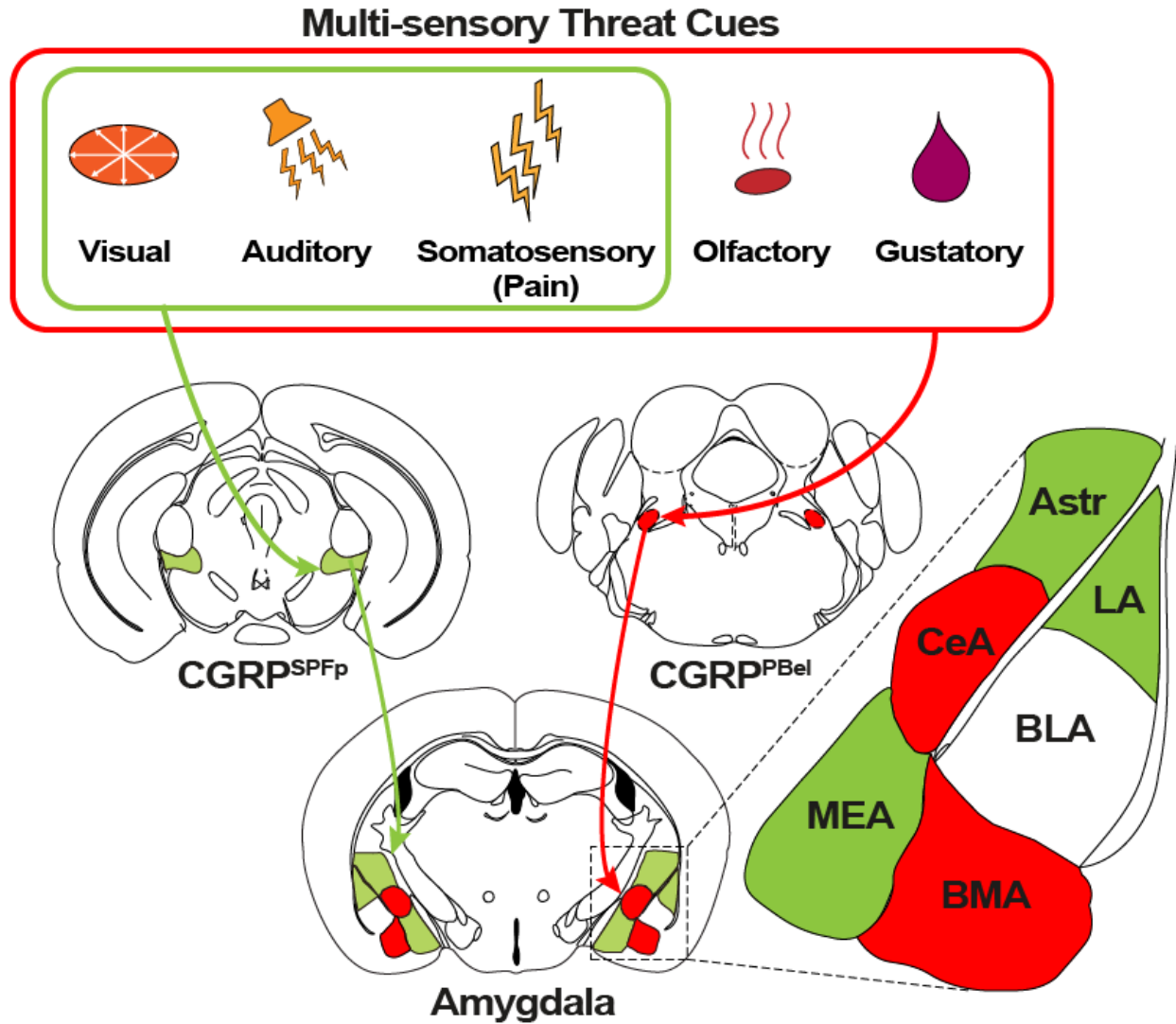
1562 (L) pIC; EPSC: 3.63 ± 0.49 ms (n = 15 cells), IC IPSC: 8.49 ± 0.83 ms (n = 8 cells). Unpaired t test (two-
1563 tailed), p < 0.0001.

1564 (M) Repeated measure two-way ANOVA showed significance in laser X group interaction ($F(2, 29) =$
1565 7.215 , p = 0.0029) and laser ($F(1, 29) = 13.24$, p = 0.0011, but not group ($F(2, 29) = 2.607$, p = 0.0910).
1566 Laser ON and was significantly larger than OFF in AStr (p < 0.001) and pIC (p < 0.05). Additionally,
1567 difference between EYFP vs Astr (p < 0.01) and EYFP vs pIC (p < 0.05) during ON period were significant.

1568 (N) EYFP: 3.842 ± 0.89 (n = 13), AStr: 14.82 ± 3.32 (n = 8), pIC: 17.94 ± 6.40 % (n = 9). One-way ANOVA
1569 showed significant (p = 0.0161). EYFP vs IC was significantly different (p < 0.05) with Tukey's multiple
1570 comparison test.

1571 (O) Repeated measure two-way ANOVA showed significance in CS X group interaction ($F(2, 27) = 3.647$,
1572 p = 0.0396) and CS ($F(1, 27) = 39.74$, p < 0.0001) but not in group ($F(2, 27) = 2.948$, p = 0.0695). CS+ was
1573 significantly larger than CS- in AStr (p < 0.05) and pIC (p < 0.0001). Moreover, difference between EYFP
1574 and pIC in CS+ was significant (p < 0.01) with Sidak's multiple comparison test.

1575



1576
1577
1578

Figure S10. Summary illustration